Centrifugal-electrostatic confinement fusion

C. A. Ordonez[1,a] and D. L. Weathers[1]

[1]*Department of Physics,*
University of North Texas,
Denton, Texas 76203, USA

(Dated: September 1, 2023)

Abstract

A model for plasma confinement is developed and applied for describing an electrically confined thermonuclear plasma. The plasma confinement model includes both an analytical approach that excludes space charge effects and a classical trajectory Monte Carlo simulation that accounts for space charge. The plasma consists of reactant ions that form a nonneutral plasma without electrons. The plasma drifts around a negatively charged electrode. Conditions are predicted for confining a deuterium-tritium plasma using a 460 kV applied electric potential difference. The ion plasma would have a 20 keV temperature, a 10^{20} m^{-3} peak density, and a 110 keV average kinetic energy per ion (including drift and thermal portions at a certain point in the plasma). The fusion energy production rate is predicted to be 10 times larger than the energy loss rate, including contributions associated with both plasma loss to electrodes and secondary electron emission. However, an approach for enhancing the fusion power density may have to be employed to realize a practical use for centrifugal-electrostatic confinement fusion.

[a] Author to whom correspondence should be addressed: cao@unt.edu.

I. INTRODUCTION

While it is not possible to produce a three-dimensional electrostatic potential well in vacuum, it is possible to use an electrostatic field as part of an ion confinement approach that includes the presence of a magnetic field and/or electrons. Examples include variations of the Penning trap,[1–4] the electron beam ion trap,[5,6] inertial-electrostatic confinement fusion,[7,8] electrostatically plugged magnetic cusps,[9] Penning fusion,[10] the Polywell,[11] the Orbitron,[12] and boundary confinement of electrons that produce a three-dimensional electrostatic potential well for confining ions.[13–16] There also exist approaches for purely electric confinement of ions without the presence of a magnetic field or electrons. Examples include electrostatic storage of ion beams,[17] and centrifugal-electrostatic traps such as the Kingdon trap and the Orbitrap.[18–22] Various applications have been reported for centrifugal-electrostatic traps.[23–29] Descriptions of the confinement physics associated with centrifugal-electrostatic traps have been based primarily on classical trajectory simulations and analyses.[30–32]

Centrifugal-electrostatic confinement is defined here as an approach for trapping charged particles (including drifting nonneutral plasmas) that requires both an effective centrifugal force and an electric force. Because a centrifugal force is not a real force, centrifugal-electrostatic confinement is a type of purely electric confinement. In the work reported in Ref. 32, a confinement model for centrifugal-electrostatic traps was developed based on defining an effective centrifugal potential energy and deriving an expression for the fraction of confined particles that follow a drifting Maxwellian velocity distribution. The derivation considered a limited range of values for one velocity component. The work presented here is intended to be self-contained and is an extension of the work presented in Ref. 32. Here, an understanding of the losses of particles and energy to surrounding structures is developed using two approaches. In addition, the scientific advances are applied for predicting the confinement of a thermonuclear plasma. It should be noted that the normalized effective potential energy and thermal speed have different definitions here than in Ref. 32. Also, the term "plasma" is used here without regard to the relative value of the Debye length.

Figure 1 shows an example of an axisymmetric configuration that may serve for providing centrifugal-electrostatic confinement of a nonneutral plasma. The illustration shows four electrodes and plasma. The plasma would be confined within a toroidal confinement volume and would experience a net drift around a section of the inner electrode, which has the

appearance of a wire in the figure. The outer electrode has the appearance of a hollow cylinder. There are also two endcap electrodes, which serve to provide axial confinement of the plasma.

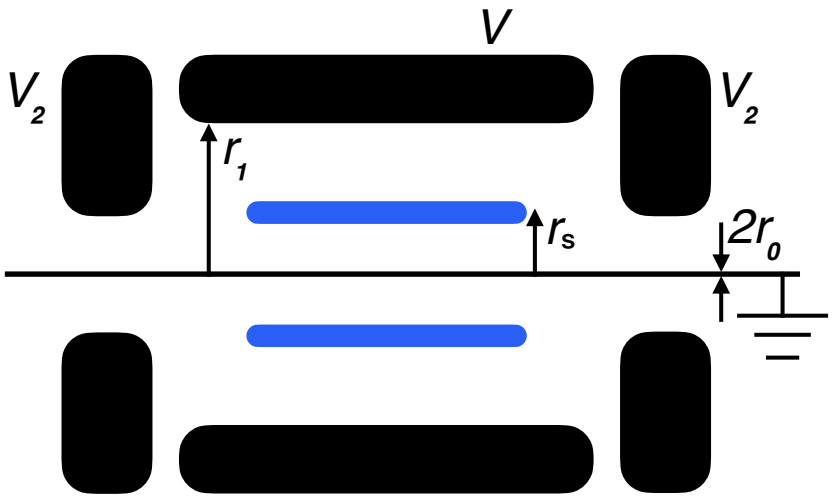

FIG. 1. Illustration showing the cross section of an axisymmetric electrode system (black) for confining a nonneutral plasma (blue). The electrodes consist of an inner electrode with radius r_0 and zero electrostatic potential, an outer electrode with inner radius r_1 and electrostatic potential V, and two endcap electrodes that each have electrostatic potential V_2. The plasma consists of particles that pass radially back and forth through the radius r_s. Normalized parameters are used including $\rho_1 = r_1/r_0$, $\rho_s = r_s/r_0$, and $\nu = qV/T$, where T is the plasma temperature in energy units, and q is the charge of a plasma particle. The figure is not to scale.

Section II provides a discussion of considerations and basic assumptions used to develop the description of centrifugal-electrostatic plasma confinement reported here. Sections III and IV provide an analytical approach for describing centrifugal-electrostatic confinement within a system qualitatively similar to that shown in Fig. 1. The analytical approach includes some integrals that are evaluated numerically. The collisionless and low-density

limits are taken in Sec. III, while collisions are considered in Sec. IV. The confinement model in Secs. III and IV is applied in Sec. V for describing the confinement of a fusion plasma in the low-density limit. Section VI provides a computational approach for describing radial plasma confinement accounting for the effect of space charge. The computational approach incorporates a classical trajectory Monte Carlo simulation. The confinement model in Secs. IV and VI is applied in Sec. VII for describing the confinement of a fusion plasma, including the effect of space charge. Section VIII provides a discussion of the results found. Concluding remarks are in Sec. IX.

II. CONFINEMENT MODEL DEVELOPMENT CONSIDERATIONS

A. Radial Particle Confinement

Equations that govern the radial motion of a particle in a centrifugal-electrostatic plasma trap are considered here in Subsec. II A. The plasma confinement system is treated as being axisymmetric and as consisting of a coaxial pair of cylindrical electrodes of infinite length. Axial confinement is not treated, with the assumption that the axial motion of a particle is decoupled from motion in the other dimensions. A cylindrical coordinate system is defined with coordinates (r, θ, z), and with associated unit vectors $(\hat{\boldsymbol{r}}, \hat{\boldsymbol{\theta}}, \hat{\boldsymbol{z}})$. The z axis of the coordinate system is located along the axis of symmetry of the system. A plasma particle in the system is treated classically as a point charge that represents a positive ion. Unless noted otherwise, the particle is considered to be affected only by a static and axisymmetric electric field produced by the electrodes and by the space charge of a quiescent plasma.

The acceleration of a particle in the system as a function of time t is

$$\boldsymbol{a}(t) = \left[r''(t) - r(t)\,\theta'(t)^2\right]\,\hat{\boldsymbol{r}}(t) + \left[r(t)\,\theta''(t) + 2\,r'(t)\,\theta'(t)\right]\,\hat{\boldsymbol{\theta}}(t). \tag{1}$$

An absence of force and acceleration in the azimuthal direction is satisfied by a constant angular momentum about the z axis, $L = mr^2\theta'$, where m is the mass of the particle. Substituting $\theta' = L/(mr^2)$ into the centripetal acceleration term and applying Newton's second law yields an equation of motion,

$$mr''(t) = \frac{L^2}{mr(t)^3} - \frac{qV}{r(t)\ln(r_1/r_0)} + qE_p\left[r(t)\right]. \tag{2}$$

Here, q is the particle's charge and V is the difference in electric potential between the outer electrode having an inner radius r_1 and the inner electrode having an outer radius r_0. The first term on the right with an r^{-3} dependence is a short-range outward centrifugal force. The second term on the right with an r^{-1} dependence is a longer-range inward electric force that would be due to the radial electric field produced by the electrodes without plasma present. In the last term on the right, the function $E_p(r)$ is defined such that the last two terms on the right together provide an electric force that accounts for a confined plasma's space charge.

The centrifugal force, $\boldsymbol{F}_C(r) = L^2/(mr^3)\hat{\boldsymbol{r}}$, can be treated as a conservative force, because its curl is zero, $\boldsymbol{\nabla} \times \boldsymbol{F}_C = \boldsymbol{0}$. A centrifugal potential energy $U_C(r)$ is defined such that $\boldsymbol{F}_C(r) = -\boldsymbol{\nabla} U_C(r)$. The centrifugal potential energy can be written as $U_C(r) = U_{C0} + L^2/(2mr^2)$, where U_{C0} is an arbitrary constant. Let $\phi(r)$ denote the electric potential, let $U(r) = q\phi(r) + U_C(r)$ be defined as the effective potential energy of the particle, and let $K_r = \frac{1}{2}mv_r^2$ be referred to as the radial kinetic energy of the particle, where $v_r = r'(t)$. The effective energy for radial motion is defined as the sum of radial kinetic energy and effective potential energy, $E_{\text{eff}} = K_r + U$. A particle is considered to be lost from confinement if it reaches either the inner electrode at $r = r_0$ or the outer electrode at $r = r_1$. The effective energy E_{eff} is a conserved quantity. Therefore, a particle in the system will remain confined, so long as the particle's effective energy remains smaller than the effective potential energy at each electrode, $E_{\text{eff}} < U(r_0)$ and $E_{\text{eff}} < U(r_1)$.

Suppose that a confined plasma particle passes radially back and forth through a radial coordinate denoted r_s. If only the effects considered here in Subsec. II A are present, the particle's radial kinetic energy is the same at the time of each pass, $K_r(r_s) = E_{\text{eff}} - U(r_s)$. The two conditions for confinement of the particle can be expressed as $K_r(r_s) < U(r_0) - U(r_s)$ and $K_r(r_s) < U(r_1) - U(r_s)$. If both conditions are satisfied by the particle, both conditions will continue to be satisfied indefinitely, if additional effects (e.g., the effects of collisions) are not present.

B. Assumptions

In the work presented here, it is assumed that axial motion is not coupled to motion in the other dimensions. When the effects of collisions are accounted for, it is assumed

that the collisional mean-free-path is large compared to plasma dimensions. With an effective potential energy well providing radial particle confinement and an electric potential energy well providing axial particle confinement, it is assumed that collisions tend to cause a confined plasma to approach a drifting Maxwellian velocity distribution at a certain radial point $r = r_s$ in the plasma, and that nearly all confined plasma particles pass back and forth through the radial coordinate r_s. No assumptions are made regarding a phase-space distribution that would describe a confined plasma, and such a distribution has not been found. Effects that can cause a decrease of the angular momentum of the system of confined particles are not considered here.

A process for efficiently loading a plasma into a centrifugal-electrostatic trap is not developed in the present work. However, a brief discussion of a possible process is provided in this paragraph. It is assumed that previously reported methods, such as those described in Refs. 19, 21, 22, 24, and 28, provide a suitable basis for developing new methods, as needed, for loading a plasma (e.g., a fusion plasma) into a centrifugal-electrostatic trap. It is speculated that a focused ion beam could be used to inject ions through a hole in the outer electrode, while the applied electric potential difference V between the outer and inner electrodes is increasing. At the point of entry, the injected ions would have a sufficiently small radial kinetic energy $K_r(r_1)$ to be captured by the changing applied potential. The azimuthal velocity component would be chosen such that each ion has a desired angular momentum L at the point of entry. The axial velocity component at the point of entry would be chosen with the expectation that axially counterstreaming ions will activate the two-stream instability, which, together with collisions, converts kinetic energy associated with axial motion into thermal energy. The plasma would initially be loaded in a high orbit, with nearly all particles passing back and forth through a radial coordinate r_s. Radial compression by increasing the applied potential difference V would then be used to change the value of r_s to a desired value.

C. Comparisons With Magnetic Plasma Confinement

Consider a confined plasma with an ion mean-free-path that is large compared to the plasma's dimensions. For a quasineutral plasma that is confined only magnetically, collisions that cause a change of a plasma ion's orbit in configuration space may lead to the loss of

the ion. In contrast, for a nonneutral ion plasma that is confined only electrically, with such confinement treated as a square potential energy well, collisions that cause a change of a plasma ion's velocity may lead to the loss of the ion. The ion loss rate may be modeled as collision-based diffusion in configuration space for one case and collision-based diffusion in velocity space for the other case.

In a quasineutral plasma that is confined only magnetically, the presence of electrons may provide a number of important energy loss mechanisms, including synchrotron radiation, bremsstrahlung radiation, and cross-magnetic-field energy transport that may occur at a rate that is larger than that due to collisions alone. Such energy loss mechanisms are negligible or absent in a nonneutral ion plasma that is electrically confined.

Variations of the Penning trap employ both a magnetic field and an electric field for confining nonneutral plasmas.[1,2] With such traps, low temperature antimatter is routinely confined using superconducting magnets for days or even years.[3] In Penning traps, a plasma state referred to as global thermal equilibrium is possible that is characterized by sheer-free rotation associated with a cross-magnetic-field drift.[2] In contrast, the same equilibrium does not occur without the presence of a magnetic field. A rotating-wall technique can be used to maintain the rotational drift in Penning traps.[2] It is not clear if a technique for maintaining a rotational drift is possible for a nonneutral plasma confined without the presence of a magnetic field.

A Penning trap could potentially confine a nonneutral fusion plasma without electrons. However, a density limit, which is named after Brillouin[33], would severely limit the fusion power density. For example, the Brillouin density limit for 2.5 amu ions in a 20 T magnetic field is 4.3×10^{17} m^{-3}, which may be considered too small for the fusion power density to be of practical use. The Brillouin density limit is a disciplinary issue, specific to Penning traps. The approach considered here for confining a nonneutral fusion plasma is not subject to the Brillouin density limit. However, there exist a number of interdisciplinary issues associated with generating a fully nonneutral fusion plasma.[34]

III. CONFINEMENT IN THE COLLISIONLESS AND LOW-DENSITY LIMITS

A. Confinement Configuration

An axisymmetric plasma confinement system is considered to consist of a cylindrical inner electrode located within a hollow cylindrical outer electrode, with both electrodes much longer than the radius of the outer electrode. A drifting nonneutral plasma is considered to be located between the electrodes. A model describing the confinement of such a plasma is developed for a region far from the axial ends of the electrodes.

A cylindrical coordinate system with radial, azimuthal, and axial coordinates, (r, θ, z), is defined in configuration space, with the z axis coincident with the axis of symmetry of the plasma confinement system. An imaginary cylindrical surface is defined that is located at radial coordinate $r = r_s$ and that has a finite axial length. The imaginary surface is much farther from each axial end than the radius of the outer electrode and is much longer than axial plasma variations.

The plasma confinement model presented here applies to plasma particles that orbit the inner electrode in one azimuthal direction and that pass radially back and forth through the imaginary surface. The region of applicability is treated as being axisymmetric, i.e., no θ dependence, and without axial variations, i.e., no z dependence. Thus, only one cylindrical coordinate, the radial coordinate r, is used. For convenience, plasma confinement is referred to as occurring for particles that pass radially back and forth through a single point $r = r_s$, with the single point representing the imaginary surface.

B. Drifting Maxwellian Velocity Distribution

A Cartesian coordinate system is defined in velocity space for describing the velocities of confined particles as they pass through the single point r_s, which has a fixed value. Such plasma particles are considered to nearly follow a drifting Maxwellian velocity distribution at r_s. The drifting Maxwellian velocity distribution normalized to one is written as

$$f_v(v_r, v_\theta, v_z) = \frac{1}{(\sqrt{\pi} v_{\rm th})^3} \exp\left[-\frac{v_r^2 + (v_\theta - v_d)^2 + v_z^2}{v_{\rm th}^2} \right]. \tag{3}$$

Here, v_r, v_θ, v_z are radial, azimuthal, and axial velocity components, which form a Cartesian set of coordinates in velocity space, v_d is the azimuthal drift velocity, $v_{\rm th} = \sqrt{2T/m}$ is the

thermal speed, T is the plasma temperature in energy units, and m is the mass of a plasma particle. Hereafter, the symbol w denotes velocity normalized by the thermal speed. For example, $w_z = v_z/v_{\rm th}$. The drifting Maxwellian normalized-velocity distribution is

$$f_w(w_r, w_\theta, w_z) = \pi^{-3/2} e^{-\left[w_r^2 + (w_\theta - w_d)^2 + w_z^2\right]}. \tag{4}$$

Confined particles are considered to have limited ranges of normalized-velocity component values specified by $w_{z,\rm max}$, $w_{r,\rm max}$, $w_{\theta,\rm min}$ and $w_{\theta,\rm max}$. Particles are not considered to be confined for which any of the following inequalities are satisfied: $|w_z| > w_{z,\rm max}$, $|w_r| > w_{r,\rm max}$, $w_\theta < w_{\theta,\rm min}$, or $w_\theta > w_{\theta,\rm max}$. The fraction of particles that follow the drifting Maxwellian normalized-velocity distribution is evaluated as

$$f_p = \int_{w_{\theta,\rm min}}^{w_{\theta,\rm max}} \int_{-w_{r,\rm max}}^{w_{r,\rm max}} \int_{-w_{z,\rm max}}^{w_{z,\rm max}} f_w(w_r, w_\theta, w_z) dw_z dw_r dw_\theta. \tag{5}$$

The distribution $f_w(w_r, w_\theta, w_z)$ is normalized, such that $f_p = 1$ if the limits $w_{z,\rm max} \to \infty$, $w_{r,\rm max} \to \infty$, $w_{\theta,\rm min} \to -\infty$, and $w_{\theta,\rm max} \to \infty$ are taken. Integration over two normalized velocity components yields,

$$f_p = \pi^{-1/2} \int_{w_{\theta,\rm min}}^{w_{\theta,\rm max}} e^{-(w_\theta - w_d)^2} \mathrm{erf}\left(w_{z,\rm max}\right) \mathrm{erf}\left(w_{r,\rm max}\right) dw_\theta, \tag{6}$$

where erf is the error function. Expressions for $w_{z,\rm max}$, w_d, $w_{r,\rm max}$, $w_{\theta,\rm min}$, and $w_{\theta,\rm max}$ are now obtained.

C. Normalized Velocity Expressions

The electric potential between the inner and outer cylindrical electrodes can be written as

$$\phi(\rho) = \phi_0 + \frac{V \ln(\rho)}{\ln(\rho_1)}. \tag{7}$$

Here, $\rho = r/r_0$ is the radial coordinate normalized by r_0, the radius of the inner electrode's outer surface, $\rho_1 = r_1/r_0$ is the normalized radius of the outer electrode's inner surface, which has radius r_1, ϕ_0 is an arbitrary additive constant, and $V = \phi(\rho_1) - \phi(1)$ is the difference in electric potential between the outer and inner cylindrical electrodes. Hereafter, $\phi_0 = \phi(1) = 0$ is used, by defining the electric potential to be zero at the inner electrode.

Axial confinement is treated by assuming that a particle located at a normalized radial coordinate $\rho_s = r_s/r_0$, where the electric potential is $\phi(\rho_s)$, is not confined if the particle can

travel axially to reach an endcap electrode. The endcap electrodes are considered to be held at an electric potential equal to V_2. Axial motion is considered to be decoupled from motion in the other two dimensions, and a particle at ρ_s with a z component of velocity larger in magnitude than $v_{z,\max}$ is assumed to not be confined axially, where $\frac{1}{2}mv_{z,\max}^2 = qV_2 - q\phi(\rho_s)$, or equivalently,

$$w_{z,\max} = \sqrt{\nu\left(\frac{V_2}{V} - \frac{\ln(\rho_s)}{\ln(\rho_1)}\right)}. \tag{8}$$

Here, $\nu = qV/T$, and q is the charge of a confined particle.

The effective centrifugal potential energy of a particle between the inner and outer cylindrical electrodes can be written as $U_C(\rho) = U_{C0} + L^2/(2mr_0^2\rho^2)$. Here, U_{C0} is an arbitrary additive constant, and L is the particle's angular momentum about the z axis. The effective centrifugal potential energy is defined to be zero at the inner electrode, which requires the additive constant to be $U_{C0} = -L^2/(2mr_0^2)$. The total effective potential energy of the particle is $U(\rho) = q\phi(\rho) + U_C(\rho)$. With this, a normalized effective potential energy is written as

$$u(\rho) = \frac{\nu\ln(\rho)}{\ln(\rho_1)} - \ell^2\left(1 - \frac{1}{\rho^2}\right), \tag{9}$$

where $u = U/T$ and $\ell = \sqrt{L^2/(2mr_0^2T)}$. Figure 2 shows three plots of $u(\rho)/\nu$ with $\rho_1 = 100$ and with $\ell^2/\nu = 0.5, 1.0, 1.5$. Each plot shows how an effective potential energy well can form.

A confined particle that does not interact with other particles would have an angular momentum and associated value of ℓ that are conserved quantities. The conserved quantity ℓ can be written in terms of the normalized azimuthal velocity component, w_θ, for a particle located at the normalized radial coordinate, $\rho = \rho_s$, as

$$\ell = \rho_s w_\theta. \tag{10}$$

All confined particles are considered to orbit the inner electrode by traveling in the same direction, with $w_\theta > 0$ for each particle. As a particle moves radially, the value of w_θ varies with ρ, such that ℓ remains constant. However, in the approach used here, the value of w_θ is that for a particle as it passes through a single fixed point, ρ_s, with $1 < \rho_s < \rho_1$. A distribution of w_θ values is associated with many particles that have a distribution of velocities, as each particle passes through the normalized radial coordinate, ρ_s.

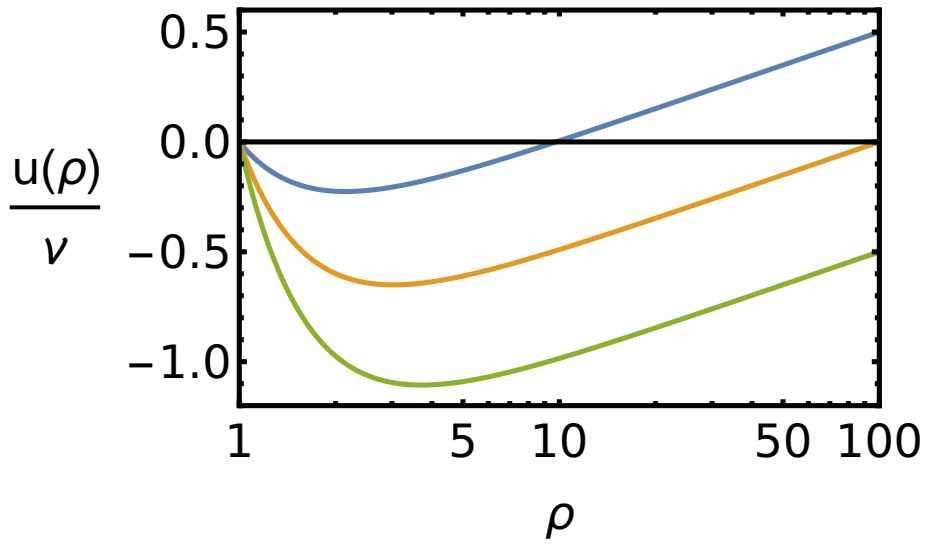

FIG. 2. Plots of $u(\rho)/\nu$ with $\rho_1 = 100$ and with $\ell^2/\nu = 0.5$ (top blue line), $\ell^2/\nu = 1.0$ (middle yellow line), and $\ell^2/\nu = 1.5$ (bottom green line).

The normalized drift velocity is specified as $w_d = \alpha_d w_c$, where α_d is a chosen constant, and w_c is the value of w_θ at which a particle with $w_r = w_z = 0$ experiences a circular orbit of normalized radius ρ_s. A circular orbit occurs when there is a radial balance of electric and effective centrifugal forces, which occurs at a minimum value of $u(\rho)$. Setting $w_c = w_\theta = \ell/\rho_s$ under the condition, $u'(\rho)|_{\rho=\rho_s} = 0$, yields

$$w_c = \sqrt{\frac{\nu}{2\ln(\rho_1)}}. \tag{11}$$

The differences, $u(1) - u(\rho_s)$ and $u(\rho_1) - u(\rho_s)$, represent normalized effective potential energy barriers that might keep a particle at ρ_s from reaching the inner electrode and outer electrode, respectively. If $u(1) \neq u(\rho_1)$, one of the two barriers will be smaller than the other. Setting $w_{\theta\delta} = w_\theta = \ell/\rho_s$ under the condition, $u(1) = u(\rho_1)$, gives

$$w_{\theta\delta} = \sqrt{\frac{\nu}{[1 - (1/\rho_1^2)]\,\rho_s^2}}. \tag{12}$$

If $w_\theta < w_{\theta\delta}$ then $u(1) - u(\rho_s) < u(\rho_1) - u(\rho_s)$, and particles with a normalized radial velocity component larger in magnitude than $w_{r,\max,0} = \sqrt{u(1) - u(\rho_s)}$ are assumed to not

be confined radially. Alternatively, if $w_\theta > w_{\theta\delta}$ then $u(1) - u(\rho_s) > u(\rho_1) - u(\rho_s)$, and particles with a normalized radial velocity component larger in magnitude than $w_{r,\max,1} = \sqrt{u(\rho_1) - u(\rho_s)}$ are assumed to not be confined radially. The two expressions for $w_{r,\max}$ are equivalently written as

$$w_{r,\max,0} = w_{r,\max,0}(w_\theta) = \sqrt{(\rho_s^2 - 1)\, w_\theta^2 - \frac{\nu \ln(\rho_s)}{\ln(\rho_1)}} \tag{13}$$

for $w_\theta < w_{\theta\delta}$, and

$$w_{r,\max,1} = w_{r,\max,1}(w_\theta) = \sqrt{\left(\frac{\rho_s^2}{\rho_1^2} - 1\right) w_\theta^2 + \nu \left[1 - \frac{\ln(\rho_s)}{\ln(\rho_1)}\right]} \tag{14}$$

for $w_\theta > w_{\theta\delta}$.

A normalized effective potential energy barrier only exists in the radially inward direction for a particle passing through ρ_s if $u(1) > u(\rho_s)$. Setting $w_{\theta,\min} = w_\theta = \ell/\rho_s$ under the condition, $u(1) = u(\rho_s)$, requires

$$w_{\theta,\min} = \sqrt{\frac{\nu \ln(\rho_s)}{(\rho_s^2 - 1)\ln(\rho_1)}}. \tag{15}$$

In a similar way, a normalized effective potential energy barrier only exists in the radially outward direction for a particle passing through ρ_s if $u(\rho_1) > u(\rho_s)$. Setting $w_{\theta,\max} = w_\theta = \ell/\rho_s$ under the condition, $u(\rho_1) = u(\rho_s)$, requires

$$w_{\theta,\max} = \sqrt{\frac{\nu}{1 - (\rho_s^2/\rho_1^2)} \left(1 - \frac{\ln(\rho_s)}{\ln(\rho_1)}\right)}. \tag{16}$$

D. Normalized Average Loss Kinetic Energy

Diffusion in velocity space due to the cumulative effect of many Coulomb collisions is considered to cause particle velocities to gradually change until particles barely escape confinement by being able to reach the top of an effective potential energy barrier located at an electrode. Three expressions for the normalized average loss kinetic energy are obtained for particles that barely escape confinement in the radially inward direction (by reaching the inner electrode), in the radially outward direction (by reaching the outer electrode), and in an axial direction (by reaching an endcap electrode), respectively. For each of the three cases, a particle at ρ_s would barely escape confinement if $|w_r| = w_{r,\max,0}(w_\theta)$, $|w_r| = w_{r,\max,1}(w_\theta)$,

or $|w_z| = w_{z,\max}$, respectively. The kinetic energy of a particle that reaches a loss boundary is equal to the kinetic energy at ρ_s plus the difference between the electric potential energies at ρ_s and at the boundary. For each of the three cases, the kinetic energy of a particle that reaches a loss boundary is

$$K_0 = \frac{1}{2}mv_{r,\max,0}^2 + \frac{1}{2}mv_\theta^2 + \frac{1}{2}mv_z^2 + q\phi(\rho_s) - q\phi(1), \tag{17}$$

$$K_1 = \frac{1}{2}mv_{r,\max,1}^2 + \frac{1}{2}mv_\theta^2 + \frac{1}{2}mv_z^2 + q\phi(\rho_s) - q\phi(\rho_1), \tag{18}$$

or

$$K_2 = \frac{1}{2}mv_r^2 + \frac{1}{2}mv_\theta^2 + \frac{1}{2}mv_{z,\max}^2 + q\phi(\rho_s) - qV_2, \tag{19}$$

respectively. The three normalized averages are defined as $\kappa_0 = \langle K_0 \rangle_0 / T$, $\kappa_1 = \langle K_1 \rangle_1 / T$, and $\kappa_2 = \langle K_2 \rangle_2 / T$, where $\langle\ \rangle_i$ is an average taken in velocity space. The subscripts 0, 1, and 2 on the averages serve to indicate that there are different restrictions on velocity values. For example, $w_{r,\max}$ has been separated into two parts, $w_{r,\max,0}(w_\theta)$ and $w_{r,\max,1}(w_\theta)$, which are applicable for $w_{\theta,\min} < w_\theta < w_{\theta\delta}$ and $w_{\theta\delta} < w_\theta < w_{\theta,\max}$, respectively. Each of the three normalized averages, κ_0, κ_1, or κ_2, is obtained for the fraction of particles at ρ_s that follow the drifting Maxwellian normalized-velocity distribution, except with $|w_r| = w_{r,\max,0}(w_\theta)$, $|w_r| = w_{r,\max,1}(w_\theta)$, or $|w_z| = w_{z,\max}$, respectively.

For a particle that has barely reached the inner electrode by travelling radially inward, the average loss kinetic energy is evaluated as

$$\langle K_0 \rangle_0 = \frac{\int_{w_{\theta,\min}}^{w_{\theta\delta}} \int_{-w_{z,\max}}^{w_{z,\max}} K_0 e^{-\left[(w_\theta - w_d)^2 + w_z^2\right]} dw_z dw_\theta}{\int_{w_{\theta,\min}}^{w_{\theta\delta}} \int_{-w_{z,\max}}^{w_{z,\max}} e^{-\left[(w_\theta - w_d)^2 + w_z^2\right]} dw_z dw_\theta}. \tag{20}$$

The normalized average loss kinetic energy is

$$\kappa_0 = \left\langle \rho_s^2 w_\theta^2 + w_z^2 \right\rangle_0 = \frac{1}{2} + \rho_s^2 \left(\frac{1}{2} + w_d^2 + \eta_0 \right) - \frac{w_{z,\max} e^{-w_{z,\max}^2}}{\sqrt{\pi}\,\mathrm{erf}\left(w_{z,\max}\right)}, \tag{21}$$

where

$$\eta_0 = \frac{\left(w_d + w_{\theta,\min}\right) e^{-\left(w_d - w_{\theta,\min}\right)^2} - \left(w_d + w_{\theta,\delta}\right) e^{-\left(w_d - w_{\theta,\delta}\right)^2}}{\sqrt{\pi}\left[\mathrm{erf}\left(w_d - w_{\theta,\min}\right) - \mathrm{erf}\left(w_d - w_{\theta,\delta}\right)\right]}. \tag{22}$$

The inner electrode is now considered to be negatively charged, and a charged particle that reaches the inner electrode is now considered to be a positive ion. Each time an ion reaches the inner electrode, the emission of secondary electrons may occur. Let δ denote the secondary electron emission coefficient, which is defined here as the average number

of electrons emitted from the inner electrode per incident ion. Electrons emitted from the inner electrode are accelerated radially outward and can be expected to reach the outer electrode with a kinetic energy approximately equal to $e\phi(\rho_1) = qV/Z = \nu T/Z$, where e is the magnitude of an electron's charge, and Z is an ion's atomic number. It is assumed for the present work that every ion has the same atomic number and is fully ionized. To account for the loss of energy associated with secondary electron emission, the expression for κ_0 is modified to be

$$\kappa_0 = \frac{1}{2} + \rho_s^2\left(\frac{1}{2} + w_d^2 + \eta_0\right) - \frac{w_{z,\max}e^{-w_{z,\max}^2}}{\sqrt{\pi}\mathrm{erf}\left(w_{z,\max}\right)} + \frac{\nu\delta}{Z}, \tag{23}$$

For a particle that has barely reached the outer electrode by travelling radially outward, the average loss kinetic energy is evaluated as

$$\left\langle K_1\right\rangle_1 = \frac{\int_{w_{\theta\delta}}^{w_{\theta,\max}}\int_{-w_{z,\max}}^{w_{z,\max}} K_1 e^{-\left[(w_\theta - w_d)^2 + w_z^2\right]} dw_z dw_\theta}{\int_{w_{\theta\delta}}^{w_{\theta,\max}}\int_{-w_{z,\max}}^{w_{z,\max}} e^{-\left[(w_\theta - w_d)^2 + w_z^2\right]} dw_z dw_\theta}. \tag{24}$$

The normalized average loss kinetic energy is

$$\kappa_1 = \left\langle \frac{\rho_s^2 w_\theta^2}{\rho_1^2} + w_z^2 \right\rangle_1 = \frac{1}{2} + \frac{\rho_s^2}{\rho_1^2}\left(\frac{1}{2} + w_d^2 + \eta_1\right) - \frac{w_{z,\max}e^{-w_{z,\max}^2}}{\sqrt{\pi}\mathrm{erf}\left(w_{z,\max}\right)}, \tag{25}$$

where

$$\eta_1 = \frac{\left(w_d + w_{\theta\delta}\right)e^{-\left(w_d - w_{\theta\delta}\right)^2} - \left(w_d + w_{\theta,\max}\right)e^{-\left(w_d - w_{\theta,\max}\right)^2}}{\sqrt{\pi}\left[\mathrm{erf}\left(w_d - w_{\theta\delta}\right) - \mathrm{erf}\left(w_d - w_{\theta,\max}\right)\right]}. \tag{26}$$

For a particle that has barely reached an endcap electrode by travelling axially, the average loss kinetic energy is evaluated as

$$\left\langle K_2\right\rangle_2 = \frac{\int_{w_{\theta,\min}}^{w_{\theta,\max}}\int_{-w_{r,\max}(w_\theta)}^{w_{r,\max}(w_\theta)} K_2 e^{-\left[(w_\theta - w_d)^2 + w_r^2\right]} dw_r dw_\theta}{\int_{w_{\theta,\min}}^{w_{\theta,\max}}\int_{-w_{r,\max}(w_\theta)}^{w_{r,\max}(w_\theta)} e^{-\left[(w_\theta - w_d)^2 + w_r^2\right]} dw_r dw_\theta}. \tag{27}$$

The normalized average loss kinetic energy is

$$\kappa_2 = \left\langle w_r^2 + w_\theta^2\right\rangle_2 = \left\langle w_r^2\right\rangle + \left\langle w_\theta^2\right\rangle = \kappa_r + \kappa_\theta, \tag{28}$$

where the normalized average particle kinetic energies associated with radial motion and azimuthal motion at ρ_s are

$$\kappa_r = \frac{\int_{w_{\theta,\min}}^{w_{\theta,\max}} e^{-\left(w_\theta - w_d\right)^2}\left[\frac{1}{2}\mathrm{erf}\left(w_{r,\max}\right) - \pi^{-1/2}w_{r,\max}e^{-w_{r,\max}^2}\right] dw_\theta}{\sqrt{\pi}f_p/\mathrm{erf}\left(w_{z,\max}\right)} \tag{29}$$

and

$$\kappa_\theta = \frac{\int_{w_{\theta,\min}}^{w_{\theta,\max}} w_\theta^2 e^{-\left(w_\theta - w_d\right)^2}\mathrm{erf}\left(w_{r,\max}\right) dw_\theta}{\sqrt{\pi}f_p/\mathrm{erf}\left(w_{z,\max}\right)}, \tag{30}$$

respectively. Each of the two numerators has an integral over w_θ that is evaluated by dividing the integral into two parts. For the first part, $w_{r,\max} = w_{r,\max,0}(w_\theta)$, and the integration limits are $w_{\theta,\min}$ to $w_{\theta\delta}$. For the second part, $w_{r,\max} = w_{r,\max,1}(w_\theta)$, and the integration limits are $w_{\theta\delta}$ to $w_{\theta,\max}$. The integral associated with f_p is also divided into two parts, as shown in the next subsection.

The normalized average particle kinetic energy associated with axial motion motion at ρ_s is

$$\kappa_z = \left\langle w_z^2 \right\rangle = \frac{\int_{-w_{z,\max}}^{w_{z,\max}} w_z^2 e^{-w_z^2} dw_z}{\int_{-w_{z,\max}}^{w_{z,\max}} e^{-w_z^2} dw_z} = \frac{1}{2} - \frac{w_{z,\max} e^{-w_{z,\max}^2}}{\sqrt{\pi}\mathrm{erf}(w_{z,\max})}. \tag{31}$$

The normalized average particle kinetic energy associated with full motion at ρ_s is

$$\kappa = \kappa_r + \kappa_\theta + \kappa_z. \tag{32}$$

E. Confinement Fractions

The fraction of particles that follow the drifting Maxwellian normalized-velocity distribution, being confined by both a radial effective potential energy well and an axial potential energy well, is

$$f_p = \frac{\mathrm{erf}\left(w_{z,\max}\right)}{\sqrt{\pi}} \Bigg(\int_{w_{\theta,\min}}^{w_{\theta\delta}} e^{-(w_\theta - w_d)^2} \mathrm{erf}\left[w_{r,\max,0}(w_\theta)\right] dw_\theta + \int_{w_{\theta\delta}}^{w_{\theta,\max}} e^{-(w_\theta - w_d)^2} \mathrm{erf}\left[w_{r,\max,1}(w_\theta)\right] dw_\theta \Bigg). \tag{33}$$

This fraction, f_p, is used to obtain expressions for three other fractions, denoted f_0, f_1, and f_2, to develop separate descriptions of particle confinement in the radially inward, radially outward, and axial directions, respectively. The three fractions, f_0, f_1, and f_2, are each defined as the fraction of particles that follow the drifting Maxwellian normalized-velocity distribution excluding only particles that would not be confined either radially inward, or radially outward, or axially, respectively. Taking the limits $w_{z,\max} \to \infty$, $w_{r,\max,1} \to \infty$, and $w_{\theta,\max} \to \infty$, yields

$$f_0 = \frac{1}{2}\left[1 + \mathrm{erf}\left(w_d - w_{\theta\delta}\right)\right] + \frac{1}{\sqrt{\pi}} \int_{w_{\theta,\min}}^{w_{\theta\delta}} e^{-(w_\theta - w_d)^2} \mathrm{erf}\left[w_{r,\max,0}(w_\theta)\right] dw_\theta. \tag{34}$$

Taking the limits $w_{z,\max} \to \infty$, $w_{r,\max,0} \to \infty$, and $w_{\theta,\min} \to -\infty$, yields

$$f_1 = \frac{1}{2}\mathrm{erfc}\left(w_d - w_{\theta\delta}\right) + \frac{1}{\sqrt{\pi}} \int_{w_{\theta\delta}}^{w_{\theta,\max}} e^{-(w_\theta - w_d)^2} \mathrm{erf}\left[w_{r,\max,1}(w_\theta)\right] dw_\theta. \tag{35}$$

Here, erfc is the complementary error function. Taking the limits $w_{r,\max,0} \to \infty$, $w_{r,\max,1} \to \infty$, $w_{\theta,\min} \to -\infty$, and $w_{\theta,\max} \to \infty$, yields

$$f_2 = \mathrm{erf}\left(w_{z,\max}\right). \tag{36}$$

For each fraction, a value of one corresponds to perfect confinement of the thermal distribution at ρ_s, while a value of zero corresponds to no confinement. Assuming that particles are not confined for which $|w_r| > w_{r,\max,0}(w_\theta)$, $|w_r| > w_{r,\max,1}(w_\theta)$, or $|w_z| > w_{z,\max}$, the fraction f_p of particles that follow the drifting Maxwellian normalized-velocity distribution is related to those of f_i by $f_p = f_2(f_0 + f_1 - 1)$.

Particles that are lost in the radially inward direction (by reaching the inner electrode) have $w_\theta < w_{\theta\delta}$, while particles that are lost in the radially outward direction (by reaching the outer electrode) have $w_\theta > w_{\theta\delta}$. The fractional portions of f_p associated with $w_\theta < w_{\theta\delta}$ and $w_\theta > w_{\theta\delta}$ are

$$f_{r0} = \frac{\mathrm{erf}\left(w_{z,\max}\right)}{f_p\sqrt{\pi}} \int_{w_{\theta,\min}}^{w_{\theta\delta}} e^{-(w_\theta - w_d)^2} \mathrm{erf}\left[w_{r,\max,0}(w_\theta)\right] dw_\theta \tag{37}$$

and

$$f_{r1} = \frac{\mathrm{erf}\left(w_{z,\max}\right)}{f_p\sqrt{\pi}} \int_{w_{\theta\delta}}^{w_{\theta,\max}} e^{-(w_\theta - w_d)^2} \mathrm{erf}\left[w_{r,\max,1}(w_\theta)\right] dw_\theta, \tag{38}$$

respectively. The sum of the two fractions is equal to one, $f_{r0} + f_{r1} = 1$.

IV. COLLISIONS

The rate at which the plasma density changes is evaluated by using Eq. (13) from Ref. 35, which applies for plasma confinement in the presence of a magnetic mirror and a square potential energy well in one dimension. The expression is 12% larger in magnitude than the corresponding equation in Ref. 36 for a mirror ratio of one and for confined ions. The expression is repeated here with the mirror ratio set equal to one, without a negative sign used to indicate particle loss, and with an integral evaluated in analytical form:

$$\frac{dn}{dt} = \frac{4n}{\sqrt{\pi}c^2\tau_0} \sqrt{\frac{1}{1+c^2}} \frac{e^{-\omega_i}}{\ln\left(4c^{-2}+2\right)} \frac{1}{\omega_i} \left(1 + \frac{\sqrt{\pi}e^{\omega_i}\mathrm{erfc}(\sqrt{\omega_i})}{2\sqrt{\omega_i}}\right). \tag{39}$$

Here, ω_i is the height of a particle-confining potential energy barrier normalized by the plasma temperature, $\tau_0 = \sqrt{mT^3}/(\sqrt{2}\pi n k_C^2 e^4 \lambda)$ for singly charged particles, $c = \sqrt{2}$ for ions, λ is the Coloumb logarithm, $k_C = 1/(4\pi\epsilon_0)$ is the Coulomb force constant in SI units, and ϵ_0 is the vacuum permittivity. The value of ω_i is directly related to the fraction f_i of particles that follow a Maxwellian velocity distribution, excluding particles not confined by the square potential energy well,

$$\omega_i = \omega_i(f_i) = \left[\text{erf}^{-1}\left(f_i\right)\right]^2. \tag{40}$$

Equations (39) and (40) are used here for separate descriptions of particle losses in the radially inward, radially outward, and axial directions. The magnitude of the rate at which the plasma density decreases due to particle losses associated with collisional scattering is evaluated as

$$\dot{n}_\ell = \sum_{i=0}^{2} f_{ri} \left.\frac{dn}{dt}\right|_{\omega_i = \omega_i(f_i)}. \tag{41}$$

Here, f_{r0} and f_{r1} represent the fractional portions of particles that can only be lost in the radially inward direction or outward direction, respectively. There is no corresponding restriction for particle loss in the axial direction, and the definition, $f_{r2} = 1$, is made for use in the summation. Also, f_i is the fraction of particles that follow a drifting Maxwellian velocity distribution, excluding particles not confined in the radially inward direction ($i = 0$), radially outward direction ($i = 1$), or an axial direction ($i = 2$).

The magnitude of the rate at which energy is incident on electrodes due to particle losses associated with collisional scattering is evaluated as

$$P_\ell = \sum_{i=0}^{2} P_i = \sum_{i=0}^{2} \kappa_i T f_{ri} \left.\frac{dn}{dt}\right|_{\omega_i = \omega_i(f_i)}. \tag{42}$$

Here, κ_i is the normalized average loss kinetic energy for a particle that has barely reached the top of an effective potential energy barrier by reaching the inner electrode ($i = 0$), the outer electrode ($i = 1$), or an endcap electrode ($i = 2$).

V. APPLICATION OF ANALYTICAL MODEL IN THE LOW-DENSITY LIMIT

Confinement of a $T = 20$ keV deuterium-tritium plasma is now considered (with $m = 2.5$ amu and $Z = q/e = 1$) in the low-density limit. Let Q denote the ratio of the fusion power

density to the energy loss power density,

$$Q = \frac{P_f}{P_\ell}. \tag{43}$$

Here, P_ℓ is given by Eq. (42). The fusion power density is evaluated as

$$P_f = \frac{1}{4} E_f n^2 \langle \sigma v \rangle_f , \tag{44}$$

where $E_f = 17.6$ MeV is the energy released per deuterium-tritium fusion reaction, $\langle \sigma v \rangle_f = 4.33 \times 10^{-22}$ m^3 /s is the fusion reactivity,[37] and n is the ion density (including both ion species with equal densities). For obtaining the value of $\langle \sigma v \rangle_f$, the plasma velocity distribution is approximated as Maxwellian in the plasma's rest frame, by requiring that the fraction of particles that follow a drifting Maxwellian velocity distribution be close in value to one ($f_p \approx 1$). The confinement model is expected to decrease in accuracy with smaller values of f_p. The condition $f_p > 0.9$ is satisfied for all applicable results reported here, unless noted otherwise. The Coulomb logarithm is approximated as having a constant value of $\lambda = 20$, and Q becomes independent of the ion density n. The value, $\alpha_d = 1$ is chosen, so that the drift velocity is equal to the particle speed for a circular orbit.

With fixed plasma parameters, Q is a function of five parameters consisting of ρ_1, ρ_s, V, δ, and V_2. Table I shows the results of an optimization procedure with the secondary electron emission coefficient taken to be $\delta = 1$, and the electric potential at each endcap electrode taken to be the same as that at the outer electrode, $V_2 = V$. For each value of ρ_1, the value of ρ_s is found to two significant figures such that Q has a maximum value, and simultaneously, the value of V is adjusted to equal V_{10}. V_{10} is defined to be the smallest value of V to two significant figures for which $Q > 10$ is predicted.

Parameter values are chosen for a base case consisting of $\rho_1 = 60$, $\rho_s = 10$, $V = 460$ kV, $\delta = 1$, and $V_2 = V$. For the base case, the ratio of the fusion power density to the energy loss power density is predicted to be $Q = 10.3$ in the low-density limit. Other predictions include the following: the confinement fractions, $f_0 = 0.968$, $f_1 = 0.978$, $f_2 = 1.00$, $f_p = 0.946$, $f_{r0} = 0.0139$, and $f_{r1} = 0.986$; the average energy loss per ion that reaches the inner electrode, $\langle K_0 \rangle_0 = 831$ keV, the outer electrode, $\langle K_1 \rangle_1 = 11.8$ keV, and an endcap electrode, $\langle K_2 \rangle_2 = 74.6$ keV; and the average ion kinetic energy associated with radial motion, $\langle K_r \rangle = 9.75$ keV, azimuthal motion, $\langle K_\theta \rangle = 64.8$ keV, axial motion, $\langle K_z \rangle = 10.0$ keV, and full motion, $\langle K \rangle = 84.6$ keV. The average energy loss per ion that

TABLE I. Results from an optimization procedure, with a secondary electron emission coefficient, $\delta = 1$, and with an electric potential at each endcap electrode equal to that at the outer electrode, $V_2 = V$. Here, $\rho_1 = r_1/r_0$ and $\rho_s = r_s/r_0$, where r_1 is the inner radius of the outer electrode, r_0 is the outer radius of the inner electrode, and r_s is a radius where the plasma approximately follows a drifting Maxwellian velocity distribution. Also, V_{10} is the smallest electric potential at the outer electrode (with the inner electrode at zero potential) for the confinement model to predict $Q > 10$. Q is the ratio of the fusion power density to the energy loss power density. Confinement of a $T = 20$ keV deuterium-tritium plasma is considered.

ρ_1	ρ_s	V_{10} (kV)	f_p
12.5	4.1	820	0.98
25	6.3	590	0.96
50	9.5	480	0.95
100	14	410	0.93
200	21	360	0.92
1000	48	290	0.88

reaches the inner electrode is predicted to be much larger than that associated with reaching the outer or endcap electrodes, because of a number of contributions. Recall that part of the energy loss is defined to be associated with the release of secondary electrons from the inner electrode. An average of $\delta = 1$ secondary electron is assumed to be released per incident ion and to gain an energy, $\delta eV = 460$ keV, before reaching the outer electrode. The energy, $\delta eV = 460$ keV, is the largest contribution. The second largest contribution is the energy, $e\phi(\rho_s) = eV \ln(\rho_s)/\ln(\rho_1) = 259$ keV, that each ion gains traveling from $\rho = \rho_s$ to the inner electrode at $\rho = 1$. The remaining contributions consist of the kinetic energy associated with radial motion at ρ_s that barely leads to ion loss and the average kinetic energies associated with azimuthal and axial motion at ρ_s.

Figures 3 to 7 show the value of Q as a function of one parameter, while setting the other four parameters equal to their base case values. Figure 3 shows that Q has a maximum at approximately $\rho_1 = 60$, with other parameters set equal to their base case values. At ρ_1 values less than 60, the distance between plasma at ρ_s and the outer electrode is reduced. As a result, increased losses to the outer electrode cause Q to decrease. Similarly, at ρ_1

values greater than about 60, increased losses to the inner electrode cause Q to decrease.

Figure 4 shows that Q has a maximum at approximately $\rho_s = 10$ with other parameters set equal to their base case values. At ρ_s values less than 10, the separation between ρ_s and the inner electrode is reduced. As a result, increased losses to the inner electrode cause Q to decrease. Similarly, at ρ_s values greater than about 10, the separation between ρ_s and the outer electrode is reduced, and increased losses to the outer electrode cause Q to decrease.

Figure 5 shows the dependence that Q has on the applied electric potential difference V. Figure 5 shows that Q increases with V, with base case values used for the other four parameters. Figure 6 indicates that Q has a weak dependence on the endcap electric potential when $V_2 > 0.8V$. Figure 7 shows that secondary electron emission at the inner electrode causes Q to decrease as δ increases, and that $Q > 15$ is predicted in the limit, $\delta \to 0$.

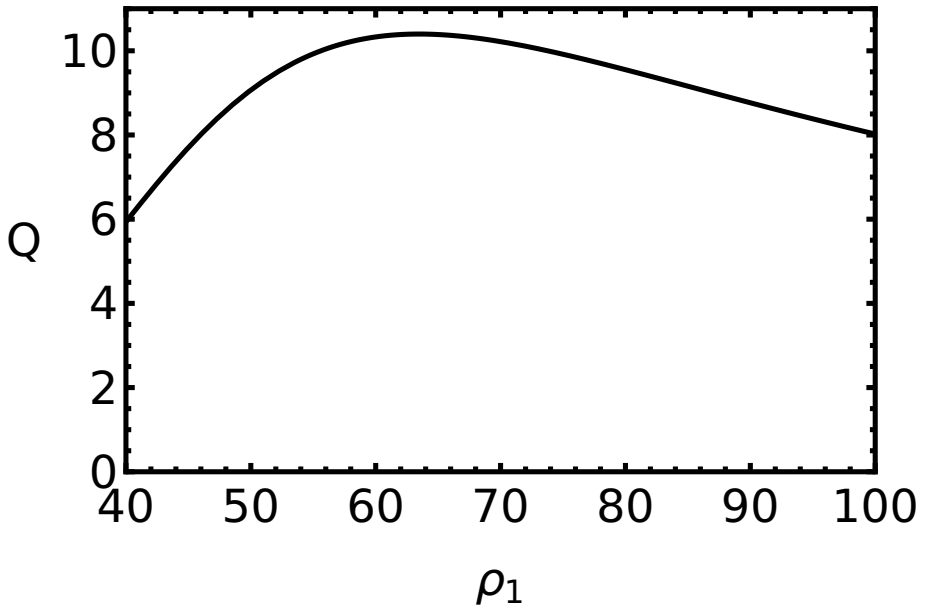

FIG. 3. Plot of Q versus ρ_1 with $\rho_s = 10$, $V = 460$ kV, $\delta = 1$, and $V_2 = V$.

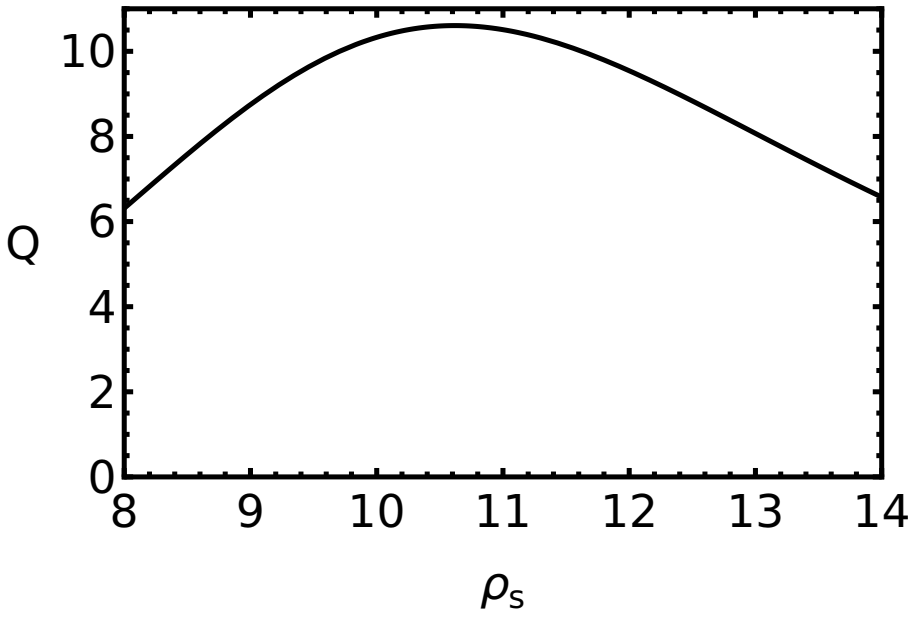

FIG. 4. Plot of Q versus ρ_s with $\rho_1 = 60$, $V = 460$ kV, $\delta = 1$, and $V_2 = V$.

VI. CLASSICAL TRAJECTORY MONTE CARLO SIMULATION

A. Initial Conditions

Equation (2) is numerically solved to simulate the radial motion of one particle at a time without accounting for collisions. An iterative technique is described below that is used to obtain $E_p(r)$, such that the results apply even at higher plasma densities. Each simulated trajectory starts at time $t = 0$ at a radial coordinate, $r(0) = r_s$. The initial velocity components of each particle are sampled from a drifting Maxwellian velocity distribution,

$$f(v_{rs}, v_{\theta s}) = \frac{m}{2\pi T} \exp\left(-\frac{m[v_{rs}^2 + (v_{\theta s} - v_d)^2]}{2T}\right), \tag{45}$$

which is normalized to one as written. Here, $r'(0) = v_{rs}$ is the initial radial velocity component, $v_{\theta s}$ is the initial azimuthal velocity component, v_d is the azimuthal drift velocity of the plasma, and T is the plasma temperature in energy units. The initial velocity components, v_{rs} and $v_{\theta s}$, are Cartesian coordinates in velocity space, each with a value between $-\infty$

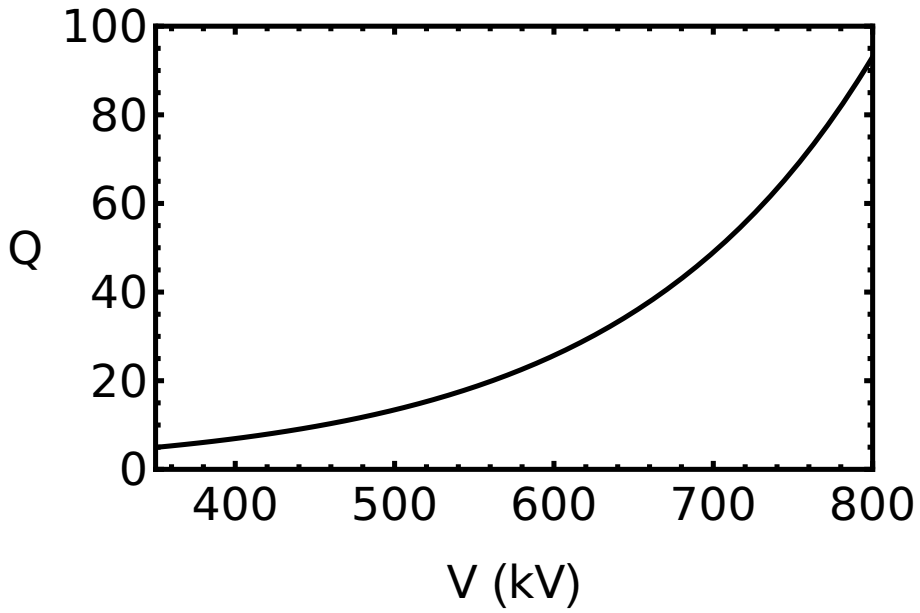

FIG. 5. Plot of Q versus V with $\rho_1 = 60$, $\rho_s = 10$, $\delta = 1$, and $V_2 = V$.

and ∞. Computationally, each of the two velocity components is sampled from a normal distribution with a standard deviation equal to $\sqrt{T/m}$ and with a mean equal to zero for the radial component or with a mean equal to v_d for the azimuthal component. The angular momentum of each particle is calculated using $L = mr_s v_{\theta s}$.

B. Ending Conditions

Each trajectory simulation ends at a time $t_{\max}$, which is defined to occur at the earliest time for which any of the following three conditions is satisfied: (1) The particle reaches the inner electrode, $r(t_{\max}) = r_0$. (2) The particle reaches the outer electrode, $r(t_{\max}) = r_1$. (3) The particle reaches the starting coordinate, $r(t_{\max}) = r_s$, for a third time (which requires passing through the starting coordinate exactly one time). The simulated particle is considered to be lost in the first two cases and to be confined in the third case. For the third case, a particle starts at $r = r_s$ traveling in one radial direction, reaches a radial

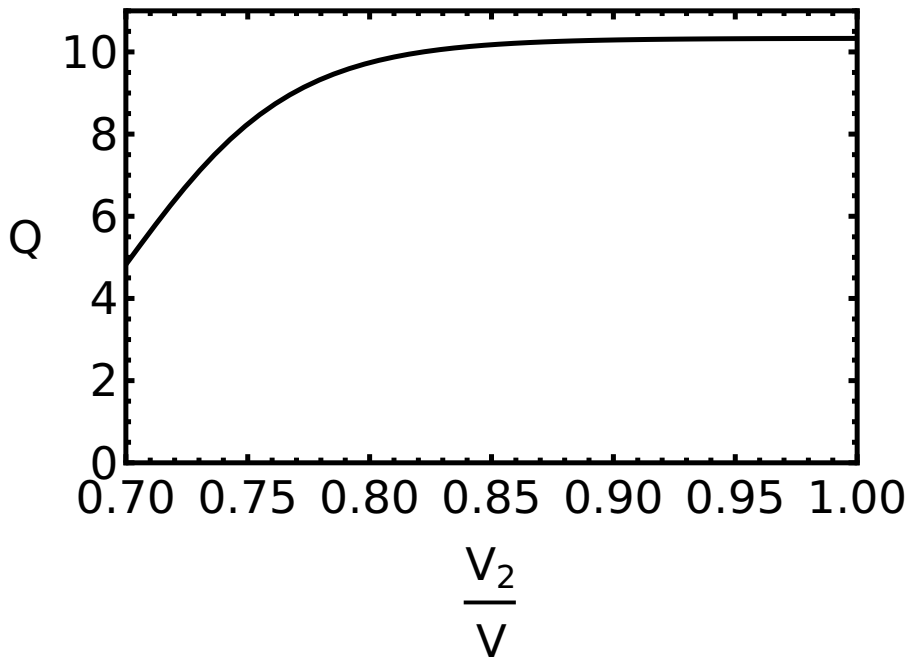

FIG. 6. Plot of Q versus V_2/V with $\rho_1 = 60$, $\rho_s = 10$, $V = 460$ kV, and $\delta = 1$.

turning point, returns to $r = r_s$ a second time and passes through, reaches a second radial turning point, and returns to $r = r_s$ a third time. A confined particle would continue to repeat such radial oscillations if the simulation is not ended.

C. Distribution of Confined Particles

For each confinement trajectory (which ends at time $t_{\max}$ at the starting coordinate r_s), N_n time values are randomly selected using $t_n = R_n t_{\max}$. Here, R_n denotes a random number that is equally likely to have any value between zero and one. A radial coordinate $r_n = r(t_n)$ is recorded for each value of t_n. For a set of confinement trajectories, the associated set of all generated r_n values represents a distribution of radial coordinates for confined particles.

The region between electrodes is divided into N_b bins of radial width, $w_b = (r_1 - r_0)/N_b$. Let N_k denote the number of r_n values within a bin labeled k that is bounded by imaginary

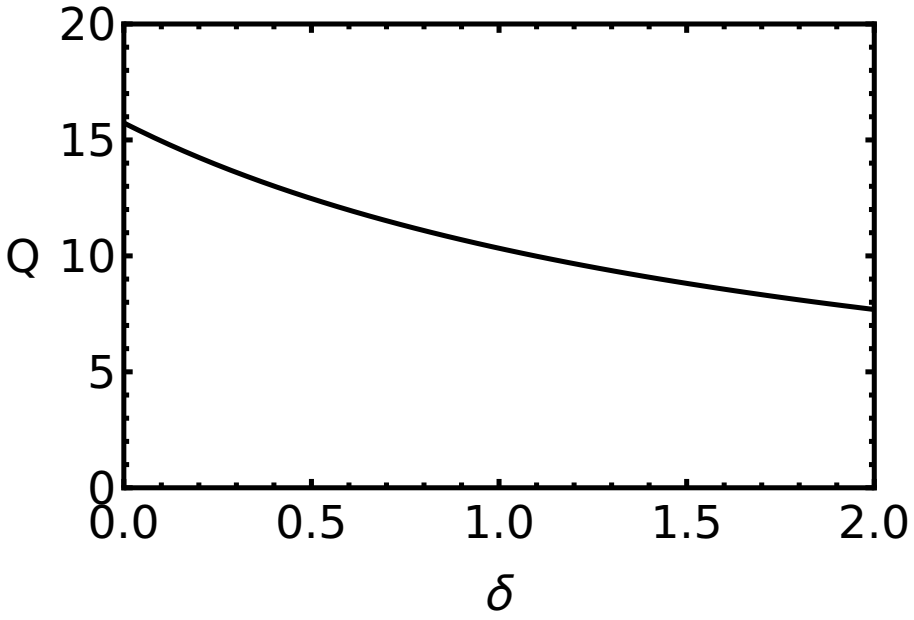

FIG. 7. Plot of Q versus δ with $\rho_1 = 60$, $\rho_s = 10$, $V = 460$ kV, and $V_2 = V$.

cylindrical surfaces at $r_0 + (k-1)w_b$ and at $r_0 + kw_b$, with $1 \leq k \leq N_b$. The radial midpoint location of the kth bin is $r_k = r_0 + (k - 0.5)w_b$. The points (r_k, N_k) represent the simulated radial distribution of confined particles. While it is possible to generate a set of N_k values with $N_n = 1$, a larger value for N_n tends to make smoother the simulated radial distribution of confined particles.

D. Plasma Density Profile

The simulated radial particle distribution N_k is used to obtain a radial plasma density profile. A constant denoted c_n is defined such that the product $c_n N_k$ represents the number of plasma particles per unit length associated with plasma in the kth bin. The plasma density n_k within each bin is approximated as constant and given by $c_n N_k = n_k \nu_k$, where

the volume per unit length of the kth bin is

$$\nu_k = \pi w_b \left[2r_0 + (2k-1)w_b\right]. \tag{46}$$

A value for the constant c_n is determined by choosing the maximum value for n_k:

$$c_n = \pi w_b \left[2r_0 + (2k_{\max}-1)w_b\right] n_{\max}/N_{\max}. \tag{47}$$

Here, $n_{\max}$ and $N_{\max}$ are the maximum values of n_k and N_k, respectively, and $k_{\max}$ is the value of k for which $N_k = N_{\max}$. Solving for the plasma density in the kth bin gives,

$$n_k = \frac{\left[2r_0 + (2k_{\max}-1)w_b\right] n_{\max} N_k}{\left[2r_0 + (2k-1)w_b\right] N_{\max}}. \tag{48}$$

With the kth bin centered at radial coordinate r_k, the points (r_k, n_k) represent the simulated radial plasma density profile for confined particles.

E. Self-Consistent Electric Field

According to Gauss' law, the electric field at radial coordinate r between the inner and outer electrodes is

$$E_r(r) = \frac{\lambda_0 + \lambda_r(r)}{2\pi\epsilon_0 r}. \tag{49}$$

Here, λ_0 is the charge per unit length on the inner electrode, λ_r is the charge per unit length of plasma located between r_0 and r, and ϵ_0 is the permittivity of free space. Defining the electric potential to be zero at the inner electrode, the electric potential at the outer electrode is

$$V = -\int_{r_0}^{r_1} E_r(r)dr = -\frac{1}{2\pi\epsilon_0}\left[\lambda_0 \ln\left(\frac{r_1}{r_0}\right) + \int_{r_0}^{r_1} \frac{\lambda_r(r)}{r} dr\right]. \tag{50}$$

Solving for λ_0 gives

$$\lambda_0 = -\lambda_v - \frac{1}{\ln(r_1/r_0)} \int_{r_0}^{r_1} \frac{\lambda_r(r)}{r} dr, \tag{51}$$

where

$$\lambda_v = \frac{2\pi\epsilon_0 V}{\ln(r_1/r_0)} \tag{52}$$

is the magnitude of the charge per unit length on the inner electrode that would occur in vacuum without plasma present. Substitution into Eq. (49) gives an equation for the radial electric field in terms of V instead of λ_0:

$$E_r(r) = -\frac{V}{r\ln(r_1/r_0)} + E_i(r), \tag{53}$$

where

$$E_i(r) = \frac{1}{2\pi\epsilon_0 r}\left(\lambda_r(r) - \frac{1}{\ln(r_1/r_0)}\int_{r_0}^{r_1}\frac{\lambda_r(r)}{r}dr\right). \tag{54}$$

Equation (53) is the radial electric field used in Eq. (2), except with $E_p(r)$ used in Eq. (2) in place of $E_i(r)$ in Eq. (53).

The plasma's charge per unit length within the kth bin is $\lambda_k = Zen_k\nu_k$, where n_k is given by Eq. (48) and ν_k is given by Eq. (46). The charge per unit length of plasma located between r_0 and a bin boundary at radial coordinate, $r_j = r_0 + jw_b$ with $1 \le j \le N_b$, is

$$\lambda_j = \sum_{k=1}^{j}\lambda_k = \frac{\pi Zew_b n_{\max}}{N_{\max}}\left[2r_0 + (2k_{\max} - 1)w_b\right]\sum_{k=1}^{j}N_k. \tag{55}$$

A boundary condition at $r_j = r_0$ is also defined as $\lambda_{j=0} = 0$. The discrete distribution given by (r_j, λ_j) for $0 \le j \le N_b$ is fit with an interpolating function, which is used as $\lambda_r(r)$ in Eq. (54) to numerically evaluate $E_i(r)$.

A self-consistent electric field is considered to be simulated when the functional dependence of $E_p(r)$ used in Eq. (2) is numerically close to the resulting function $E_i(r)$ evaluated using Eq. (54). An iterative technique is applied for finding a suitable function for $E_p(r)$. Hereafter, let $E_i(r)$ denote the function obtained during the ith iteration. Each iteration begins by using

$$E_p(r) = \omega E_{i-1}(r) + (1-\omega)E_{i-2}(r) \tag{56}$$

in Eq. (2) for running N_{tot} trajectory simulations. Here, $E_{i-1}(r)$ and $E_{i-2}(r)$ are functions found using Eq. (54) in the preceding two iterations, and ω is a chosen constant. However, for the first iteration, $E_{i-1}(r) = E_{i-2}(r) = 0$ is used, and for the second iteration, $E_{i-2}(r) = 0$ is used. A value of ω is chosen for which, $\frac{1}{2} < \omega < 1$, with larger values expected to result in faster convergence and smaller values expected to result in slower but eventually closer convergence. The convergence closeness is characterized at the end of the last iteration by calculating,

$$C_i = \left(\sum_{j=1}^{N_b}\left[E_p(r_j) - E_i(r_j)\right]^2\right)^{1/2}\left(\sum_{j=1}^{N_b}\left[E_p(r_j)\right]^2\right)^{-1/2}. \tag{57}$$

Equation (57) gives the root-mean-square difference between the values of E_p and E_i at the bin boundaries divided by the root-mean-square value of E_p at the bin boundaries. Perfect convergence to a self-consistent electric field occurs in the limits $C_i \to 0$ and $N_{\text{tot}} \to \infty$. With a finite value for N_{tot}, the value of C_i is not expected to continue to decrease in value

beyond a certain number of iterations. The chosen number of iterations is denoted $i_{\max}$ hereafter. The value of C_i is less than 0.05 for all simulation results reported here for which $i_{\max} > 1$.

VII. APPLICATION OF SIMULATION

A. Parameter Values

Parameter values have been chosen for three simulations, and the results of the three simulations are in Table II. The computational parameter values consist of the number of simulated trajectories, $N_{\text{tot}} = 5000$, the number of randomly sampled time values for each confinement trajectory, $N_n = 10$, the number of bins, $N_b = 101$, the convergence parameter, $\omega = 0.9$, and the number of iterations, $i_{\max}$, which is varied. The parameter values chosen for representing a deuterium-tritium fusion plasma consist of the ion mass, $m = 2.5$ amu, the ion charge state, $Z = 1$, the plasma temperature, $T = 20$ keV, and the maximum plasma density, $n_{\max} = 10^{20}$ m^{-3}. The plasma's drift velocity is specified as $v_d = \alpha_d v_c$, where α_d is varied, and v_c is the azimuthal speed for circular motion by a particle at radial coordinate $r = r_s$. Setting $r''(t) = 0$, $r(t) = r_s$, and $L = m r_s v_c$ in Eq. (2) and solving for v_c gives

$$v_c = \left[\frac{Ze}{m} \left(\frac{V}{\ln(r_1/r_0)} - r_s E_p(r_s) \right) \right]^{1/2} . \tag{58}$$

The value of v_c given by Eq. (58) is not the same as that given by Eq. (11), except when $i_{\max} = 1$ (with $E_p = 0$) is used. Other parameter values are for representing the trap. The electric potential applied to the outer electrode (with the inner electrode at zero potential) is chosen to be $V = 460$ kV. The radial coordinate where the plasma is simulated as having a drifting Maxwellian velocity distribution is specified as $r_s = \rho_s r_0$, where ρ_s is varied. The inner radius of the outer electrode is specified as $r_1 = \rho_1 r_0$, where $\rho_1 = 60$ is a chosen value. A numerical value is required for the inner electrode radius, and $r_0 = 0.02$ mm is chosen. The energy loss associated with secondary electron emission is included in the simulation, and the value $\delta = 1$ is chosen for the secondary electron emission coefficient. The average kinetic energy associated with motion in the z dimension is included in each simulation with the value, $\langle K_z \rangle = 10$ keV, although such motion is not simulated. Each simulation provides values for confinement fractions and average loss kinetic energies that are used in Eq. (42),

TABLE II. Results from three simulations and results from the analytical model. See the text for details.

	Analytical	Sim 1	Sim 2	Sim 3
ρ_s	10	10	10	6
α_d	1	1	1	1.2
$i_{\max}$	-	1	3	3
Q	10.3	10.6	6.64	10.2
f_0	0.968	0.969	0.971	0.981
f_1	0.978	0.982	0.952	0.973
f_p	0.946	0.952	0.924	0.954
f_{r0}	0.0139	0.0154	0.0126	0.0241
f_{r1}	0.986	0.985	0.987	0.976
$\langle K_r \rangle$ (keV)	9.75	9.47	9.47	10.0
$\langle K_\theta \rangle$ (keV)	64.8	63.7	62.3	90.0
$\langle K \rangle$ (keV)	84.6	83.2	81.7	110.
$\langle K_0 \rangle_0$ (keV)	831.	878.	877.	820.
$\langle K_1 \rangle_1$ (keV)	11.8	11.8	11.8	10.9
$P_{f,\text{avg}}$ (kW/m^3)	-	33.7	35.6	16.0
E_0 (GV/m)	-	6.38	6.44	6.09

which together with Eqs. (43) and (44), provide a value for Q.

Table II shows results from three classical trajectory Monte Carlo simulations and the results from the analytical model as described in Sec. V for the base case. The first simulation, labeled Sim 1, has parameter values $\rho_s = 10$, $\alpha_d = 1$, and $i_{\max} = 1$. The parameter values for Sim 1 are intended to correspond to those of the base case used for applying the analytical model. The analytical model includes axial losses, which are controlled by the value of V_2. The simulations do not include axial losses. However, as can be seen in Fig. 6, the effect of plasma axial losses on Q as indicated by the effect of varying V_2 on Q is not significant when V_2 has a value near that of V. Also, the effect of the plasma's space charge is excluded from the simulation when $i_{\max} = 1$, because $E_p = 0$ is used. The analytical results apply in the low-density limit, which is defined to occur when plasma space charge

effects are negligible. The value, $Q = 10.6$, from Sim 1 is less than 3% different than the value, $Q = 10.3$, from the analytical model.

The second simulation, labeled Sim 2, is the same as the first, except that $i_{\max} = 3$ is used to obtain a self-consistent electric field. The effect of the plasma's space charge is found to be significant, with Q decreasing by 37% from $Q = 10.6$ to $Q = 6.64$.

The third simulation, labeled Sim 3, also obtains a self-consistent electric field, with $i_{\max} = 3$, but with parameter values $\rho_s = 6$ and $\alpha_d = 1.2$. A process to find these values starts with evaluating Q using the values 10, 8, 6, and 4 for ρ_s using the analytical model. For each value of ρ_s, the value of α_d is found to two significant figures such that Q has a maximum value. For the four values of ρ_s, the overall maximum value of Q occurs with $\rho_s = 6$ and $\alpha_d = 1.3$ according to the analytical model. Next, simulations that obtain a self-consistent electric field are run with $i_{\max} = 3$ and $\rho_s = 6$. The value $\alpha_d = 1.2$ is found to two significant figures to maximize Q.

B. Radial Plasma Density Profile

Figure 8 shows a plot of the radial plasma density profile for Sim 3. Shown is a plot of plasma density n_k versus radial coordinate r_k. The region is divided into bins labeled k, and n_k is the density in the kth bin, while r_k is the radial coordinate of the radial center of the kth bin.

As discussed later, it is desirable for the plasma to have a narrow density profile. The plasma density profile reported here is expected to have the narrowest density profile possible for confinement of a plasma with a drifting Maxwellian velocity distribution and for the specified Sim 3 parameter values. Recall that all confined particles pass back and forth through the radial coordinate $r = r_s$. If plasma particles are also confined without passing through $r = r_s$, the plasma density profile would tend to be radially broader with $n_{\max}$ smaller for the same total space charge.

C. Sample Proportions

Let N_0, N_1, and N_p denote the number of trajectories that end at the inner electrode, the number of trajectories that end at the outer electrode, and the number of confinement

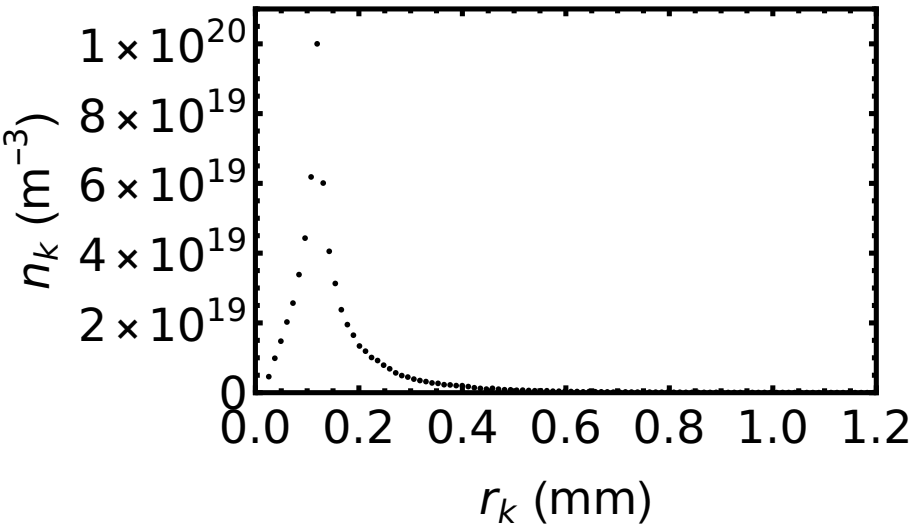

FIG. 8. Radial plasma density profile for Sim 3.

trajectories (which end at the starting coordinate), respectively. Also, let N_{r0} and N_{r1} denote the number of confinement trajectories with $v_{\theta s} \leq v_{\theta\delta}$ and $v_{\theta s} > v_{\theta\delta}$, respectively. Here, $v_{\theta s}$ is the initial azimuthal velocity component, and $v_{\theta\delta} = w_{\theta\delta} v_{\rm th}$, where the expression for $w_{\theta\delta}$ given by Eq. (12) is used, because the expression applies even with plasma space charge present.

In Table II, the values for the five confinement fractions, f_0, f_1, f_p, f_{r0}, and f_{r1}, are evaluated as sample proportions by each simulation. The sample proportion of the number of trajectories that do not end at the inner electrode is evaluated as $f_0 = (N_{\rm tot} - N_0)/N_{\rm tot}$. The sample proportion of the number of trajectories that do not end at the outer electrode is evaluated as $f_1 = (N_{\rm tot} - N_1)/N_{\rm tot}$. The sample proportion of the number of confinement trajectories is evaluated as $f_p = N_p/N_{\rm tot}$. The sample proportion of the number of confinement trajectories with $v_{\theta s} \leq v_{\theta\delta}$ is evaluated as $f_{r0} = N_{r0}/N_p$. The sample proportion of the number of confinement trajectories with $v_{\theta s} > v_{\theta\delta}$ is evaluated as $f_{r1} = N_{r1}/N_p$.

For the five sample proportions, there are five corresponding population proportions that occur in the limits, $N_{\rm tot} \to \infty$ and $N_p \to \infty$. A confidence interval is calculated for each population proportion using $f \pm (\Delta g + \Delta h)$, where Δg is associated with using a finite sample

size and Δh is introduced to account for imposing an upper limit on the simulated time each trajectory is computed. For a finite sample size, the expression $\Delta g = z^* \sqrt{[f(1-f)]/N_u}$ is used, where N_u is replaced by $N_{\rm tot}$ for f_0, f_1, and f_p, and N_u is replaced by N_p for f_{r0} and f_{r1}. (See, for example, Ref. 38 for information about the statistics.) Here, $z^* = 1.96$ is used for a 95% confidence level, assuming sample proportions are normally distributed about the corresponding population proportion. The upper limit imposed on each trajectory simulation time is chosen to be $t_m = 8r_1/v_c$ for all simulations, and all simulated trajectories that end at time t_m are excluded from the sample size. To account for an upper limit imposed on each trajectory simulation time, the expression $\Delta h = N_m/N_u$ is used. Here, N_m is the number of trajectories excluded from the sample size, which is reset to $N_{\rm tot} = N_0 + N_1 + N_p$.

The value of each confinement faction, f_0, f_1, f_p, f_{r0}, and f_{r1}, predicted by the analytical model falls within each corresponding confidence interval for Sim 1. For Sim 1, the corresponding confidence intervals are 0.969 ± 0.00558, 0.982 ± 0.00447, 0.952 ± 0.00675, 0.0154 ± 0.00440, and 0.985 ± 0.00440. For Sim 2, the confidence intervals are 0.971 ± 0.00504, 0.952 ± 0.00630, 0.924 ± 0.00777, 0.0126 ± 0.00376, and 0.987 ± 0.00376. For Sim 3, the confidence intervals are 0.981 ± 0.00517, 0.973 ± 0.00593, 0.954 ± 0.00723, 0.0241 ± 0.00590, and 0.976 ± 0.00590.

D. Kinetic Energy Averages

Values for initial radial and azimuthal velocity components, v_{rs} and $v_{\theta s}$, are sampled for each simulated trajectory. The associated average kinetic energy values in Table II are evaluated for confinement trajectories (that end at the starting coordinate) as $\langle K_r \rangle = \frac{1}{2} m \langle v_{rs}^2 \rangle$ and $\langle K_\theta \rangle = \frac{1}{2} m \langle v_{\theta s}^2 \rangle$, respectively. A velocity component for the axial dimension is not sampled. Instead, the associated average kinetic energy value is taken to be $\langle K_z \rangle = \frac{1}{2} T$. The average kinetic energy at r_s for confinement trajectories is calculated as $\langle K \rangle = \langle K_r \rangle + \langle K_\theta \rangle + \langle K_z \rangle$.

Consider a particle that is barely able to reach an electrode, because the particle's effective energy for radial motion is just barely larger than the particle's effective potential energy at the electrode. The radial kinetic energy of such a particle is approximated as being zero upon reaching the electrode, $K_r(r_i) = 0$, where $i = 0$ for the inner electrode and $i = 1$ for the outer electrode. Such an approximation is used here based on considering

diffusion in velocity space to be due to the cumulative effect of many Coulomb collisions and particle loss to be due to particles overcoming an effective potential energy barrier located at an electrode. A particle's kinetic energy upon reaching an electrode is then $K(r_i) = K_\theta(r_i) + K_z(r_i)$, where K_z would be the portion of kinetic energy associated with axial motion. The assumption is made that axial motion is decoupled from motion in other dimensions, and $K_z(r_i) = K_z(r_s)$. The assumption of conservation of angular momentum provides, $K_\theta(r_i) = (r_s/r_i)^2 K_\theta(r_s)$. The average kinetic energy of a particle incident on an electrode is then, $\langle K(r_i)\rangle_i = (r_s/r_i)^2 \langle K_\theta(r_s)\rangle_i + \langle K_z(r_s)\rangle$. The subscript i on an average is incorporated to indicate that the average only considers trajectories that can end at electrode i. The associated values for the average loss kinetic energies in Table II are evaluated by each simulation as $\langle K_0\rangle_0 = \rho_s^2 \langle K_\theta\rangle_0 + \langle K_z\rangle + eV\delta$ and $\langle K_1\rangle_1 = (\rho_s/\rho_1)^2 \langle K_\theta\rangle_1 + \langle K_z\rangle$.

The simulation does not conserve energy. As indicated in Subsec. II A, the radial kinetic energy K_r for a particle that returns to $r = r_s$ at the end of a confinement trajectory must be unchanged from when the particle started at $r = r_s$. The average difference serves as an indication of numerical inaccuracy and is less than 0.02% for trajectories that end at the starting coordinate for simulations reported here.

E. Volume Averaged Fusion Power Density

Equation (44) is used to write the fusion power density profile as

$$P_k = \frac{1}{4} E_f n_k^2 \langle \sigma v \rangle_f . \tag{59}$$

The volume averaged fusion power density in Table II is estimated as

$$P_{f,\text{avg}} = \frac{1}{\pi r_1^2} \sum_{k=1}^{N_b} P_k \nu_k = \frac{w_b}{r_1^2} \sum_{k=1}^{N_b} P_k \left[2r_0 + (2k-1)w_b\right] . \tag{60}$$

For the same total space charge, a temporal or spatial variation of plasma density tends to increase the root-mean-square value of the plasma density relative to a spatially flat and temporally constant density profile. It may be possible to increase the time- and space-averaged fusion power density by increasing the root-mean-square value of the plasma density without increasing the plasma's total space charge. One possibility is to drive time-dependent non-uniformities to large amplitudes. Another possibility is illustrated with the plasma density profile found here for Sim 3. The volume averaged plasma density is estimated for Sim 3 as

$n_{\rm avg} = \lambda_r(r_1)/(Ze\pi r_1^2) = 1.56 \times 10^{18}$ m^{-3}. The associated fusion power density is calculated using Eq. (59), except with the replacement $n_k \to n_{\rm avg}$. The result is $P_u = 738$ W/m^3, which is the power density that would occur for Sim 3 if the plasma had a spatially uniform density profile for $r < r_1$ with the total space charge unchanged. The ratio $P_{f,\rm avg}/P_u = 22$ has a value larger than one, which indicates that the plasma's nonuniform density causes the fusion power to be a factor of 22 larger than that for a uniform density with the same total space charge for Sim 3.

F. Volume Averaged Loss Power Density Associated With Field Emission

A large electric field strength E_0 at the inner electrode can cause a significant rate of electron field emission. Each emitted electron would experience an increase in kinetic energy by an amount eV as a result of traveling unimpeded to the outer electrode. Let I_e denote the magnitude of the field emission current, and let $J_e = I_e/(2\pi r_0 \ell)$ denote the corresponding field emission current density at the surface of the inner electrode. Here, ℓ denotes the axial length of the system. The energy loss rate associated with field emission is $I_e V = 2\pi r_0 \ell J_e V$. The volume averaged loss power density associated with field emission is estimated as

$$P_{e,\rm avg} = \frac{2\pi r_0 \ell J_e V}{\pi r_1^2 \ell} = \frac{2 r_0 V J_e}{r_1^2}. \tag{61}$$

Equation (7) from Ref. 39 is used to evaluate the current density J_e for cold field emission. In the cold electrode limit, Eq. (7) from Ref. 39 indicates that field emission is a function of the work function and the surface electric field. Assuming that surface impurities and surface roughness tend to enhance field emission, the ideal inner electrode may be an atomically smooth and clean wire with the highest work function possible.

High work function values that have been reported include experimental values, such as 7.42 eV,[40] and predicted values, such as 7.78 eV,[41] 7.87 eV,[42] and 9.2 eV.[43] Some pure metals have work function values reported to be between 5 eV and 6 eV including palladium (5.55 eV), platinum (5.84 eV), and gold (5.22 eV).[44] Figure 9 shows a plot of E_0 versus work function W for a volume averaged loss power density associated with field emission equal to 1 kW/m^3 for Sim 3. The value 1 kW/m^3 is 6.3% of the volume averaged fusion power density for Sim 3 and is considered here as a reasonable loss rate. Figure 9 is considered here to provide an upper limit for the possible values of E_0 for Sim 3. A value, $E_0 > 5$

GV/m, is not ruled out here as a long-term possibility. Nevertheless, it is concluded that an additional enhancement of the time- and space-averaged fusion power density may be called for, such as by intentionally driving time-dependent non-uniformities to large amplitudes.

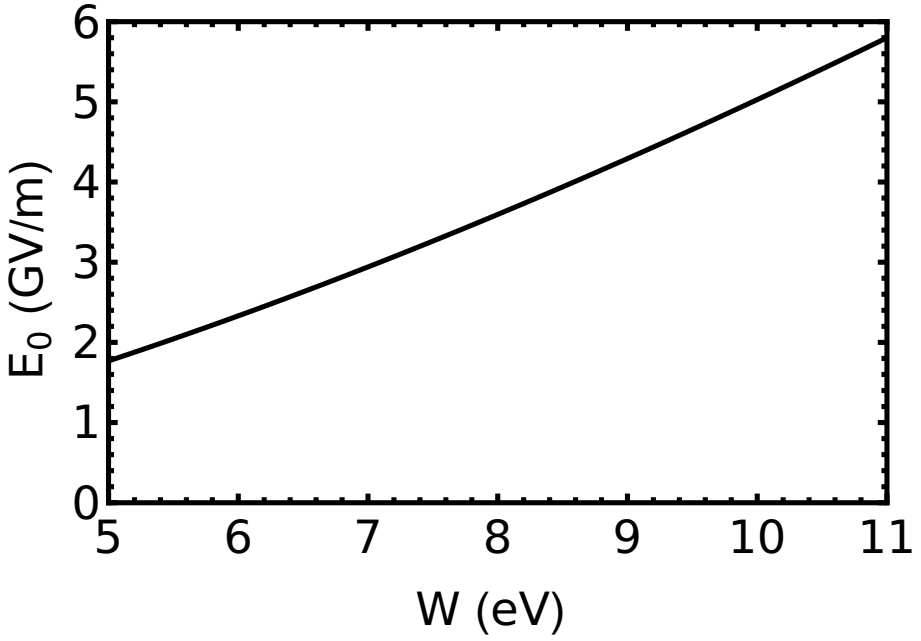

FIG. 9. Electric field at the surface of the inner electrode versus work function for a volume averaged loss power density associated with field emission equal to 1 kW/m^3 for Sim 3.

G. Energy Analysis

The volume averaged electrostatic energy density of the system is evaluated as

$$\varepsilon_{e,\text{avg}} = \frac{1}{\pi(r_1^2 - r_0^2)} \int_{r_0}^{r_1} \frac{1}{2}\epsilon_0 E_r(r)^2 2\pi r dr = \frac{\epsilon_0}{r_1^2 - r_0^2} \int_{r_0}^{r_1} E_r(r)^2\, r\, dr, \tag{62}$$

where the radial electric field $E_r(r)$ is given by Eq. (53). To obtain a value without plasma, $E_i(r) = 0$ is used, and the result for Sim 3 is $\varepsilon_{e,\text{avg}} = 317.9$ kJ/m^3. To obtain a value with plasma present, $E_i(r)$ given by Eq. (54) is used, and the result for Sim 3 is $\varepsilon_{e,\text{avg}} = 319.6$

kJ/m^3. The difference between the two values, $\Delta\varepsilon_{e,\text{avg}} = 1.7$ kJ/m^3, represents the volume averaged electrostatic energy density that would be associated with loading the system to obtain the plasma density profile shown in Fig. 8. Here, loading the system is defined as adding charged particles to the system, including negative charge added to the inner electrode in excess of the amount that would be added without adding plasma. The energy associated with particle motion is not included in $\Delta\varepsilon_{e,\text{avg}}$. The volume averaged plasma kinetic energy density (including drift and thermal portions) is estimated for Sim 3 as $\varepsilon_{p,\text{avg}} = \langle K \rangle n_{\text{avg}} = 27$ kJ/m^3. The volume averaged energy associated with loading the system for Sim 3 is $\varepsilon_{s,\text{avg}} = \Delta\varepsilon_{e,\text{avg}} + \varepsilon_{p,\text{avg}} = 28.7$ kJ/m^3, which is predominantly associated with kinetic energy.

The available fusion energy is defined here as the energy that would be produced if all plasma ions undergo fusion reactions. The volume averaged available fusion energy density of a deuterium-tritium plasma is estimated for Sim 3 as $\varepsilon_{f,\text{max}} = \frac{1}{2} E_f n_{\text{avg}} = 2.2$ MJ/m^3. Let Q_{max} denote the ratio of the available fusion energy to the energy associated with loading the system. For Sim 3, $Q_{\text{max}} = \varepsilon_{f,\text{max}}/\varepsilon_{s,\text{avg}} = 77$.

For Sim 3, $Q = P_f/P_\ell = 10.2$, where the fusion power density P_f and the energy loss power density P_ℓ are each proportional to the square of the plasma density, in the way each is evaluated here. Consequently, Q also represents the ratio of the volume averaged fusion power density to the volume averaged energy loss power density.

Equations (15) and (16) of Ref. 45 define scientific gain, $Q_{\text{sci}} = P_f/P_{\text{ext}}$, and fuel gain, $Q_{\text{fuel}} = P_f/P_{\text{abs}}$, in terms of fusion power P_f, externally applied power P_{ext}, and absorbed power $P_{\text{abs}} = \eta_{\text{abs}} P_{\text{ext}}$, where η_{abs} is the absorption efficiency. Scientific gain and fuel gain are related by $Q_{\text{sci}} = \eta_{\text{abs}} Q_{\text{fuel}}$.[45] The work presented here does not provide information that can be used to estimate a value for either η_{abs} or Q_{sci}, and only a value for Q_{fuel} is estimated for Sim 3. For applying the definition of Q_{fuel} to Sim 3, the associated terms are considered here to be volume averaged quantities. It is assumed here that a centrifugal-electrostatic confinement fusion reactor would operate using a repeating cycle consisting of a plasma loading stage, a plasma holding stage, and a plasma release stage. The absorbed power P_{abs} would be predominantly associated with the plasma loading stage, and the fusion power would be predominantly associated with the plasma holding stage. To obtain a value for Q_{fuel}, each plasma particle is treated as if it is loaded immediately before being lost, such that $P_{\text{abs}} = P_\ell$, assuming that the number of particles that undergo fusion reactions is

negligibly small compared to the number of particles that are lost. With such a treatment, $Q_{\text{fuel}} = Q = 10.2$ for Sim 3.

VIII. DISCUSSION

Confinement of a near-Maxwellian, drifting deuterium-tritium plasma is considered here, with a plasma temperature of 20 keV. The plasma consists of ions and no electrons, with each ion approximated as having a mass of 2.5 amu and with a Coulomb logarithm approximated as 20. The work presented here predicts $Q = 10$ (which is a fusion energy production rate that is 10 times larger than the rate at which energy is lost to surrounding structures) for the parameter values associated with Sim 3.

The value of the secondary electron emission coefficient δ is material-dependent and sensitive to surface conditions.[46] The value $\delta = 1$ is chosen here, by considering the data compendium reported by Ref. 46. A specific design for the endcap electrodes is not considered, and it is assumed that $V_2 = V$ is possible with a suitable design that keeps axial motion decoupled from radial and azimuthal motion. Axial motion that is decoupled from radial and azimuthal motion may also be necessary for keeping axial reflections from broadening the radial density profile (e.g., at the axial midplane).

The magnitude of the electric field at the surface of the inner electrode (E_0) cannot be too large. Too large a value of E_0 can be expected to cause significant issues associated with field emission of electrons. An upper limit for the value of E_0 can be expected to be material-dependent, sensitive to surface conditions, and affected by how high a vacuum is present. The value $E_0 = 6.1$ GV/m occurs in Sim 3. Such a value is not ruled out here as a possibility, by considering that, in Ref. 47, the electric field for a cathode spot unipolar arc is reported to be 10 GV/m. However, significant uncertainty exists with considering $E_0 = 6.1$ GV/m as a possibility. With $E_0 \ll 10$ GV/m, the present work predicts that $P_{f,\text{avg}}$ may be too small to be of practical use. The fusion power density values for future magnetic confinement fusion reactors include 600 kW/m^3 for ITER and 7 MW/m^3 for SPARC.[48,49] Such values may be significantly larger than what is possible with centrifugal-electrostatic confinement fusion.

To mitigate issues with field emission, it may be necessary to operate under conditions of ultrahigh vacuum and with special materials selected or developed for the inner electrode. It

should also be noted that if the electrode configuration illustrated in Fig. 1 is used, the electric field at the surface of the inner electrode will be larger under the endcap electrodes than at the axial midplane. For example, if the endcap electrodes are chosen to have a normalized inner radius equal to ρ_s, the electric field will increase by a factor of $\ln(\rho_1)/\ln(\rho_s) = 2.3$ for Sim 3 parameter values, under endcap electrodes that are sufficiently wide axially.

The energy flux associated with ions incident on the inner electrode is evaluated using $\delta = 0$ as

$$R_0 = \frac{r_1^2 P_{f,\text{avg}} P_0}{2 r_0 Q P_\ell}. \tag{63}$$

Here, $P_{f,\text{avg}}/Q$ gives the volume averaged energy-loss power density, $r_1^2/(2r_0)$ is the ratio of the volume associated with $r < r_1$ to the inner-electrode surface area associated with $r = r_0$, and P_0/P_ℓ is the fraction of energy incident on the inner electrode as calculated using Eq. (42). For Sim 3 parameter values, except with $\delta = 0$, the energy flux incident on the inner electrode is found to be $R_0 = 12$ W/m^2. The energy flux associated with blackbody radiation is evaluated using the Stefan-Boltzmann law, $R = \sigma T^4$, where $\sigma = 5.67 \times 10^{-8}$ W/(m^2 K^4) is the Stefan-Boltzmann constant. The blackbody-radiation energy flux from an inner electrode at approximately room temperature (300 K) is calculated to be $R = 459$ W/m^2. It is concluded for Sim 3 parameter values that the inner electrode will not heat up to a temperature significantly higher than the temperature of surrounding structures at or above room temperature, as a result of the energy flux associated with plasma ions incident on the inner electrode.

The results reported here for Sim 3 parameter values are interpreted to indicate that the volume averaged fusion power density may be too small to be of practical use, even while the fusion energy production rate is much larger than the energy loss rate to the electrodes. However, it may be possible to realize a practical use for centrifugal-electrostatic confinement fusion, if an approach can be employed for enhancing the time and space averaged fusion power density. For example, time-dependent non-uniformities that are intentionally driven to large amplitudes may increase the root-mean-square value of the plasma density and increase the time and space averaged fusion power density, without also increasing the mean value of the plasma density and the total plasma space charge.

IX. CONCLUSION

Two approaches consisting of an analytical approach and a computational approach have been developed and applied for describing an electrically confined nonneutral plasma that orbits a cylindrical electrode. The analytical approach takes the low density limit, for which the effect of space charge is negligible. The computational approach incorporates a classical trajectory Monte Carlo simulation and accounts for space charge effects. Both approaches were applied for describing confinement and loss characteristics associated with a drifting deuterium-tritium plasma that has a 20 keV temperature and a near-Maxwellian velocity distribution at one radial location. Conditions were predicted for confining a plasma using a 460 kV applied electric potential difference, such that the fusion energy production rate would exceed the energy loss rate to electrodes by a factor of 10. However, the study also indicated that the volume averaged fusion power density may be too small to be of practical use. Therefore, an approach for enhancing the volume averaged fusion power density may have to be employed to realize a practical use for centrifugal-electrostatic confinement fusion.

ACKNOWLEDGMENTS

This material is based upon work supported by the National Science Foundation under Grant No. PHY-1803047.

AUTHOR DECLARATIONS

Conflict of Interest

The authors have no conflicts to disclose.

Author Contributions

C. A. Ordonez: Conceptualization (lead); Investigation (lead); Writing - original draft (lead); D. L. Weathers: Writing - review & editing (equal); Conceptualization (supporting); Investigation (supporting).

Data Availability

The data that support the findings of this study are available within the article, from the University of North Texas Digital Library, or from an author upon reasonable request.

REFERENCES

[1] R. C. Davidson, *Physics of Nonneutral Plasmas* (World Scientific Publishing Co, 2001).

[2] D. H. E. Dubin and T. M. O'Neil, "Trapped nonneutral plasmas, liquids, and crystals (the thermal equilibrium states)," Rev. Mod. Phys. **71**, 87 (1999).

[3] J. Fajans and C. M. Surko, "Plasma and trap-based techniques for science with antimatter," Phys. Plasmas **27**, 030601 (2020).

[4] C. A. Ordonez and D. L. Weathers, "Two-species mixing in a nested Penning trap for antihydrogen trapping," Phys. Plasmas **15**, 083504 (2008).

[5] M. A. Levine, R. E. Marrs, J. R. Henderson, D. A. Knapp, and M. B. Schneider, "The electron beam ion trap: a new instrument for atomic physics measurements," Phys. Scr. **T22**, 157 (1988).

[6] F. Currell and G. Fussmann, "Physics of electron beam ion traps and sources," IEEE Trans. Plasma Sci. **33**, 1763 (2005).

[7] Y. Gu and G. H. Miley, "Experimental study of potential structure in a spherical IEC fusion device," IEEE Trans. Plasma Sci. **28**, 331 (2000).

[8] J. Hedditch, R. Bowden-Reid, and J. Khachan, "Fusion energy in an inertial electrostatic confinement device using a magnetically shielded grid," Phys. Plasmas **22**, 102705 (2015).

[9] T. J. Dolan, "Magnetic electrostatic plasma confinement," Plasma Phys. Control. Fusion **36**, 1539 (1994).

[10] D. C. Barnes, M. M. Schauer, K. R. Umstadter, L. Chacon, and G. Miley, "Electron equilibrium and confinement in a modified Penning trap and its application to Penning fusion," Phys. Plasmas **7**, 1693 (2000).

[11] J. Park, N. A. Krall, P. E. Sieck, D. T. Offermann, M. Skillicorn, A. Sanchez, K. Davis, E. Alderson, and G. Lapenta, "High-energy electron confinement in a magnetic cusp configuration,"

Phys. Rev. X **5**, 021024 (2015).

[12] M. Borghei, R. Langtry, R. McMullen, B. Riordan and R. Walker, "A compact, 300-kvdc bushing for operation under ultra-high vacuum pressure," *2022 IEEE Conference on Electrical Insulation and Dielectric Phenomena (CEIDP)*, Denver, CO, USA, pp. 471-474, (2022).

[13] J. L. Pacheco, C. A. Ordonez, and D. L. Weathers, "Space-charge-based electrostatic plasma confinement involving relaxed plasma species," Phys. Plasmas **19**, 102510 (2012).

[14] A. S. Kiester, C. A. Ordonez, and D. L. Weathers, "Ionized molecular hydrogen build-up and confinement inside the space charge of a continually resupplied electron cloud," IEEE Trans. Plasma Sci. **50**, 210 (2022).

[15] R. M. Hedlof and C. A. Ordonez, "Artificially structured boundary plasma trap," Phys. Plasmas **26**, 092509 (2019).

[16] C. A. Ordonez, "Magnetic confinement of effectively unmagnetized plasma particles," Phys. Plasmas **27**, 122501 (2020).

[17] H. T. Schmidt, "Electrostatic storage rings for atomic and molecular physics," Phys. Scr. **T166**, 014063 (2015).

[18] K. H. Kingdon, "A method for the neutralization of electron space charge by positive ionization at very low gas pressures," Phys. Rev. **21**, 408 (1923).

[19] Q. Hu, R. J. Noll, H. Li, A. Makarov, M. Hardman, and R. G. Cooks, "The Orbitrap: a new mass spectrometer," J. Mass Spectrom. **40**, 430 (2005).

[20] S. Robertson and D. Alexander, "Collective behavior of non-neutral plasma in a Kingdon trap," Phys. Plasmas **2**, 3 (1995).

[21] D. P. Moehs, D. A. Church, and R. A. Phaneuf, "Kingdon trap apparatus and technique for precise measurement of the lifetimes of metastable levels of ions," Rev. Sci. Instrum. **69**, 1991 (1998).

[22] N. Numadate, K. Okada, N. Nakamura, and H. Tanuma, "Development of a Kingdon ion trap system for trapping externally injected highly charged ions," Rev. Sci. Instrum. **85**, 103119 (2014).

[23] A. Makarov, "Electrostatic axially harmonic orbital trapping: a high-performance technique of mass analysis," Anal. Chem. **72**, 1156 (2000).

[24] R. D. Knight, "Storage of ions from laser-produced plasmas," Appl. Phys. Lett. **38**, 221 (1981).

[25] S. Robertson, "Experimental studies of charged dust particles," Phys. Plasmas **2**, 2200 (1995).

[26] D. A. Church, "Collision measurements and excited-level lifetime measurements on ions stored in Paul, Penning and Kingdon ion traps," Phys. Rep. **228**, 253 (1993).

[27] D. P. Moehs, D. A. Church, M. I. Bhatti, and W. F. Perger, "Excited-configuration metastable level lifetimes of Cl-like Mn IX and Fe X," Phys. Rev. Lett. **85**, 38 (2000).

[28] S. J. Smith, A. Chutjian, and J. A. Lozano, "Measurement of metastable lifetimes for transitions in Fe^{9+}, Fe^{10+}, and Fe^{13+}," Phys. Rev. A **72**, 062504 (2005).

[29] N. Numadate, H. Shimaya, T. Ishida, K. Okada, N. Nakamura, and H. Tanuma, "Solar wind charge exchange in laboratory - Observation of forbidden X-ray transitions," Nucl. Instrum. Methods Phys. Res. B **408**, 114 (2017).

[30] R. H. Hooverman, "Charged particle orbits in a logarithmic potential," J. Appl. Phys. **34**, 3505 (1963).

[31] R. R. Lewis, "Motion of ions in the Kingdon trap," J. Appl. Phys. **53**, 3975 (1982).

[32] C. A. Ordonez, "Effective well of a static Kingdon trap," Phys. Plasmas **15**, 072508 (2008).

[33] L. Brillouin, "A theorem of Larmor and its importance for electrons in magnetic fields," Phys. Rev. 67, 260 (1945).

[34] C. A. Ordonez, "Interdisciplinary issues associated with generating a fully non-neutral fusion plasma," in *Non-Neutral Plasma Physics V,* edited by M. Schauer, T. Mitchell, and R. Nebel, American Institute of Physics **CP692**, 267 (2003).

[35] D. L. Galbraith and T. Kammash, "Electron and ion escape over a potential barrier in a mirror field," Plasma Phys. **20**, 959 (1978).

[36] V. P. Pastukhov, "Collisional losses of electrons from an adiabatic trap in a plasma with a positive potential," Nucl. Fusion **14**, 3 (1974).

[37] H.-S. Bosch and G. M. Hale, "Improved formulas for fusion cross-sections and thermal reactivities," Nucl. Fusion **32**, 611 (1992).

[38] R. R. Subedi and J. Issos, "An improved confidence interval," Am. Intern. J. Bio. **7**, 8 (2019).

[39] H. C. Miller, "Obtaining numerical values for the elliptic emission functions used in calculating electron emission from surfaces," J. Vac. Sci. Technol. **17**, 691 (1980).

[40] J. He, J. Armstrong, P. Cong, B. Menagen, L. Igaher, A. M. Beale, L. Etgar, and D. Avnir, "Affecting an ultra-high work function of silver," Angew. Chem. Int. Ed. **59**, 4698 (2020).

[41] Y. Qian, B. Zheng, Y. Xie, J. He, J. Chen, L. Yang, X. Lu, and H. Yu, "Imparting α-borophene with high work function by fluorine adsorption: a first-principles investigation," Langmuir **37**,

11027 (2021).

[42] P. D. Taylor, D. A. Osborne, S. A. Tawfik, T. Morishita, and M. J. S. Spencer, "Tuning the work function of the silicene/4×4 Ag(111) surface," Phys. Chem. Chem. Phys. **21**, 7165 (2019).

[43] O. T. Hofmann, D. A. Egger, and E. Zojer, "Work-function modification beyond pinning: when do molecular dipoles count?," Nano Lett. **10**, 4369 (2010).

[44] S. Prada, U. Martinez, and G. Pacchioni, "Work function changes induced by deposition of ultrathin dielectric films on metals: A theoretical analysis," Phys. Rev. B **78**, 235423 (2008).

[45] S. E. Wurzel and S. C. Hsu, "Progress toward fusion energy breakeven and gain as measured against the Lawson criterion," Phys. Plasmas **29**, 062103 (2022).

[46] E. W. Thomas, "Secondary electron emission," in Data Compendium for Plasma-Surface Interactions (IAEA, Vienna, 1984), p. 94.

[47] P. Mioduszewski, "Unipolar arcing," in Data Compendium for Plasma-Surface Interactions (IAEA, Vienna, 1984), p. 105.

[48] M. Shimada, D. J. Campbell, V. Mukhovatov, M. Fujiwara, N. Kirneva, K. Lackner, M. Nagami, V. D. Pustovitov, N. Uckan, J. Wesley et al., "Progress in the ITER physics basis; Chapter 1: Overview and summary," Nucl. Fusion **47**, S1 (2007).

[49] A. J. Creely, M. J. Greenwald, S. B. Ballinger, D. Brunner, J. Canik, J. Doody, T. Fulop, D. T. Garnier, R. Granetz, T. K. Gray et al., "Overview of the SPARC tokamak," J. Plasma Phys. **86**, 865860502 (2020).

PLEASE CITE THIS ARTICLE AS DOI: 10.1063/5.0161536

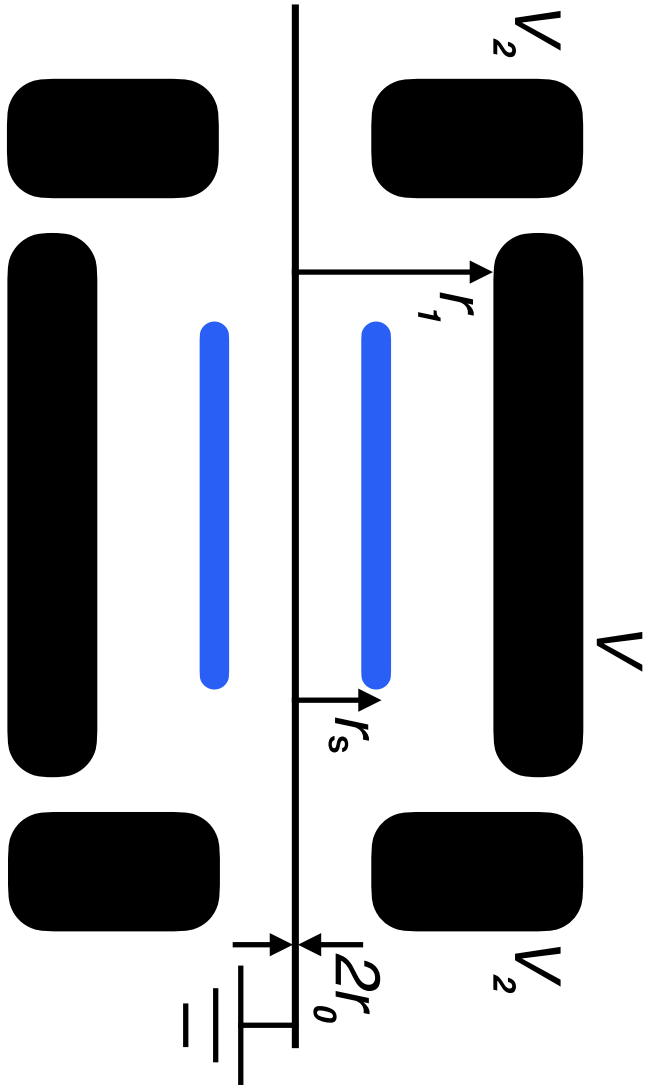

Physics of Plasmas

PLEASE CITE THIS ARTICLE AS DOI: 10.1063/5.0161536

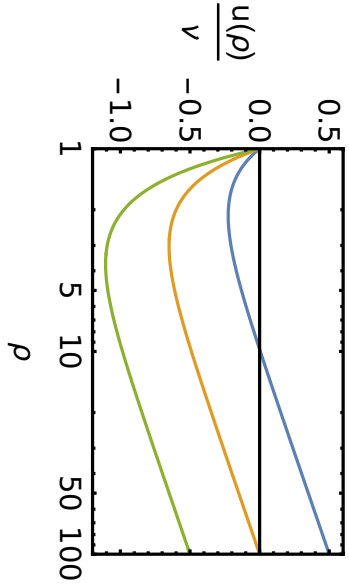

Physics of Plasmas

PLEASE CITE THIS ARTICLE AS DOI: 10.1063/5.0161536

Out[72]=

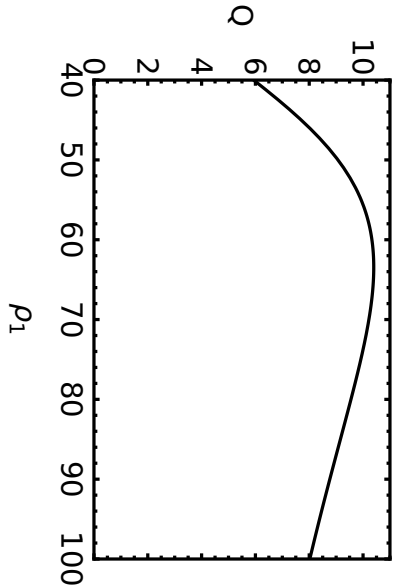

Physics of Plasmas

PLEASE CITE THIS ARTICLE AS DOI: 10.1063/5.0161536

Out[71]=

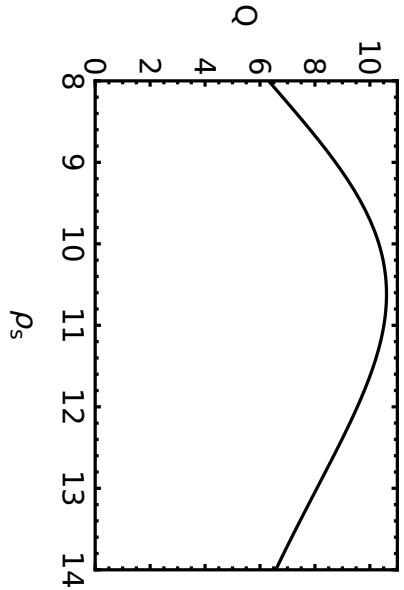

Physics of Plasmas

PLEASE CITE THIS ARTICLE AS DOI: 10.1063/5.0161536

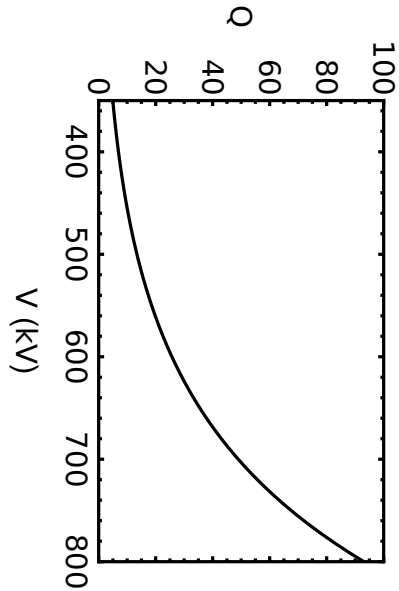

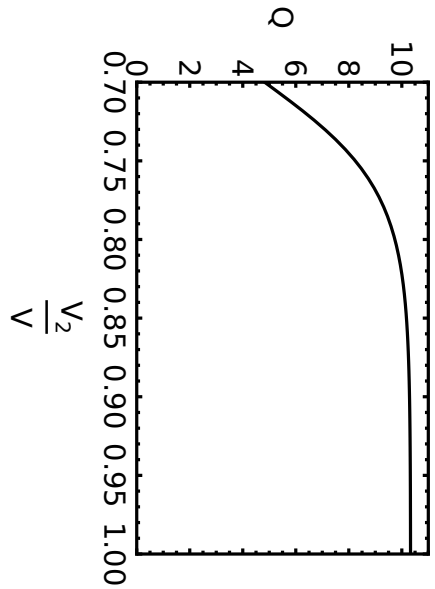

Physics of Plasmas

PLEASE CITE THIS ARTICLE AS DOI: 10.1063/5.0161536

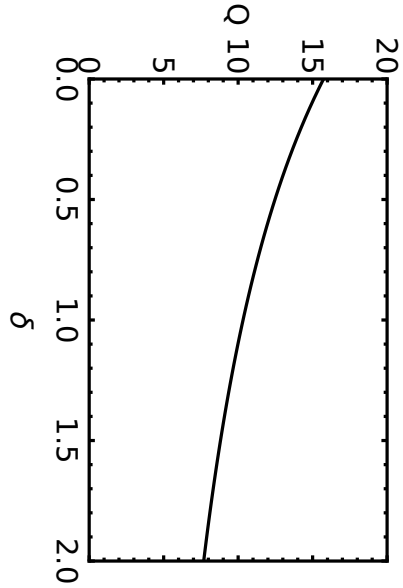

Physics of Plasmas

PLEASE CITE THIS ARTICLE AS DOI: 10.1063/5.0161536

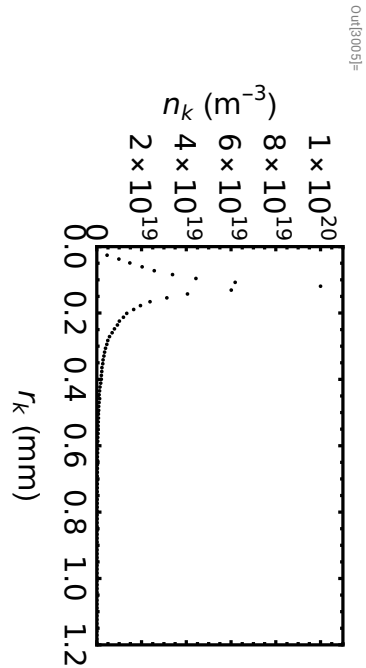

Out[32]=